HHS Public Access

Author manuscript

Nat Ecol Evol. Author manuscript; available in PMC 2024 April 08.

Published in final edited form as:

Nat Ecol Evol. 2020 June ; 4(6): 870–884. doi:10.1038/s41559-020-1157-y.

Stromal reactivity differentially drives tumour cell evolution and prostate cancer progression

Ziv Frankenstein[1,2,8], **David Basanta**[1,8], **Omar E. Franco**[3], **Yan Gao**[4], **Rodrigo A. Javier**[3], **Douglas W. Strand**[5], **MinJae Lee**[6], **Simon W. Hayward**[3,7], **Gustavo Ayala**[4,7], **Alexander R. A. Anderson**[1,7]

[1]Department of Integrated Mathematical Oncology, H. Lee Moffitt Cancer Center and Research Institute, Tampa, FL, USA

[2]Independent Researcher, New York, NY, USA

[3]Department of Surgery, NorthShore University HealthSystem Research Institute, Evanston, IL, USA

[4]Department of Pathology and Laboratory Medicine, University of Texas Health Science Center, Houston, TX, USA

[5]Department of Urology, UT Southwestern Medical Center, Dallas, TX, USA

[6]Biostatistics/Epidemiology/Research Design Core, Department of Internal Medicine, University of Texas Health Science Center, Houston, TX, USA.

[7]These authors contributed equally: Simon W. Hayward, Gustavo Ayala, Alexander R. A. Anderson

[8]These authors jointly supervised this work: Ziv Frankenstein, David Basanta

Abstract

Prostate cancer (PCa) progression is a complex eco-evolutionary process driven by the feedback between evolving tumour cell phenotypes and microenvironmentally driven selection. To better understand this relationship, we used a multiscale mathematical model that integrates data from biology and pathology on the microenvironmental regulation of PCa cell behaviour. Our data indicate that the interactions between tumour cells and their environment shape

Correspondence and requests for materials should be addressed to A.R.A.A. alexander.anderson@moffitt.org.

Author contributions

A.R.A.A., D.B., G.A. and S.W.H. developed the initial concept and obtained the funding. Z.F., D.B. and A.R.A.A. developed the mathematical model and simulation code. O.E.F., R.A.J., D.W.S. and S.W.H. conceived, designed and performed the in vitro and in vivo experiments. Y.G., M.L. and G.A. performed the statistical analysis of the clinical data. G.A. collated, stained and quantified the clinical data. Z.F. analysed the triple-stained clinical samples. Z.F., D.B., O.E.F., D.W.S., S.W.H., G.A. and A.R.A.A. co-wrote the paper.

Reporting Summary. Further information on research design is available in the Nature Research Reporting Summary linked to this article.

Competing interests

G.A. declares an interest in Stromont (a virtual company). All other authors declare no competing interests.

Extended data is available for this paper at https://doi.org/10.1038/s41559-020-1157-y.

Supplementary information is available for this paper at https://doi.org/10.1038/s41559-020-1157-y.

the evolutionary dynamics of PCa cells and explain overall tumour aggressiveness. A key environmental determinant of this aggressiveness is the stromal ecology, which can be either inhibitory, highly reactive (supportive) or non-reactive (neutral). Our results show that stromal ecology correlates directly with tumour growth but inversely modulates tumour evolution. This suggests that aggressive, environmentally independent PCa may be a result of poor stromal ecology, supporting the concept that purely tumour epithelium-centric metrics of aggressiveness may be incomplete and that incorporating markers of stromal ecology would improve prognosis.

Stromal–epithelial interactions are well-established mediators of development in most organs, including common cancer sites such as the breast, gastrointestinal tract and prostate[1-3]. In cancer, stromal alterations can both positively and negatively regulate tumour growth and progression[4-12]. Experimental models have shown that cancer-associated fibroblasts (CAFs) can promote tumorigenesis in genetically initiated benign epithelial cells. The underlying mechanisms include activation of fibroblasts, recruitment of inflammatory cells, remodelling of the extracellular matrix (ECM) and secretion of growth factors and cytokines. Interactions between subpopulations of CAFs moderate the overall stromal effect on the epithelium, suggesting potentially complex and poorly defined ecological interactions between the various components of the tumour microenvironment[9-11]. Indeed, stromal ecology is altered early in prostate cancer (PCa) development. Specifically, the stroma becomes reactive promoting tumour growth[6,7,13]. Reactive stroma includes stromal cell phenotypic switching to activated myofibroblasts, altered ECM composition, increased growth factor bio-availability, elevated protease activity, influx of tumour-associated macrophages and induction of angiogenesis[6,14]. The Gleason score is the standard grading by which PCa is diagnosed; combining this tumour-centric metric with reactive stroma grading (RSG) adds significant predictive value[8,15]. The RSG grading system is based on the amount of reactive stroma. The percentage of intratumour reactive stroma is distributed in a 4-band system where: tumours with 0–5% reactive stroma are given an RSG of 0; tumours with 5–15% reactive stroma are given an RSG of 1; and tumours with 15–50% reactive stroma are given an RSG of 2. Tumours with >50% reactive stroma are assigned RSG3. Hence, an RSG of 3 exhibits at least a 1:1 ratio of reactive stroma to epithelium. The latter is the most important category and has been dubbed stromogenic carcinoma[16]. The presence of stromogenic (or reactive stroma) carcinoma (>50% stroma[8]) in the entire tumour can predict biochemical recurrence and PCa-specific death[17]. Reactive stroma has also been correlated with tumour progression in many other cancers, such as lung, breast and skin[18].

We have focused on PCa as a model of carcinogenesis. PCa is a substantial healthcare problem due to its high incidence and mortality[19,20]. Most PCas that are diagnosed early have an indolent course. In contrast, a subgroup of PCas are so aggressive at diagnosis that surgery or radiation cannot control them[21-26]. Current prognostic standard-of-care approaches, which are tumour-centric in nature, are limited in their ability to predict these individual patterns of progression, resulting in a high level of overtreatment[27].

There is a small but growing literature on mathematical models of tumour–stroma interactions, driven by our group[28-34] and others[35,36]. However, none of these consider how stromal ecology may alter tumour evolution. Pertinent to our current work is a previous

model that employed a hybrid cellular automaton (HCA) approach to characterize the glandular architecture of prostate tissue through a layered epithelial homeostasis via growth factor signalling regulated by surrounding stroma[28].

Our previous work examined the role of reactive stroma during the early stages of PCa. While it focused on the interactions between differing degrees of stromal reactivity and the tumour, it crucially assumed a homogenous tumour population. In this study, we consider the later stages of invasive PCa and explicitly include a heterogenous tumour cell population. Our central hypothesis is that tumour evolution is shaped by stromal ecology. Building on our previous model, we now explicitly incorporate the pathological features of human PCa and have integrated mathematical and biological modelling to focus on phenotypes that elucidate disease initiation and local invasion. This allows us to investigate how the interplay between stromal components and a heterogeneous tumour epithelium modulates tumour evolution, growth and invasiveness. The predictions generated by this model were tested in biological models and cross-validated in a large cohort of human samples. We discovered that the PCa stroma exerts a selection pressure, which drives tumour heterogeneity and growth, and regulates evolution. Perhaps even more profound, the overall behaviour of the tumour in patients cannot be accurately predicted by either the cancer cell or the stromal response alone. In fact, the model predicts that the degree of stromal reactivity, when integrated with the current clinical methodology (Gleason grading with clinico-pathological parameters), significantly improves PCa prognosis predictions, which is in concordance with recent clinical studies[37]. Counter-intuitively, our mathematical model also predicts that the degree of PCa stromal reactivity inversely correlates with the evolution of the cancer cell population to more aggressive phenotypes. This suggests that aggressive, stromal-independent PCa may be an evolutionary result of poor stromal reactivity.

Results

A multiscale prostate peripheral zone model characterizes the tumour microenvironment dialogue.

To understand the role of the tumour microenvironment in PCa progression, we developed a model using an HCA paradigm[38-40] that captures this interplay. We designed the model to explicitly incorporate cellular phenotypic heterogeneity within the context of a dynamic spatio-temporal microenvironment. Each cell is considered as an individual and its behaviour emerges as a function of its phenotype under the influence of its local microenvironment. We considered six mathematically abstracted cell types: normal basal and luminal epithelial cells; tumour epithelium; native stroma, for example, muscle and fibroblasts; reactive stroma, that is, CAFs/myofibroblasts induced from normal stroma; and motile stroma, representing a generic cell with inflammatory properties. While stroma can inhibit tumour growth (in fact, we have studied the balance of pro- and antitumour roles in stroma in previous work[28]), in this study we decided to focus exclusively on the supportive role of stromal cells. While our previous work showed that stroma can inhibit tumour progression by hindering the ability of PCa cells from leaving the gland, the supportive role of stroma was shown to be more prevalent once the tumour established itself outside of the prostate gland. The physical microenvironment is described by a system of

continuum deterministic equations (see Methods), which includes growth factors (affecting cell proliferation and function), the basement membrane (representing a mechanical barrier to the glands), the ECM (structural support to intercellular communication and growth), matrix metalloproteinases (MMPs; degradation of the ECM) and empty space (assumed to be occupied by interstitial fluid; Fig. 1a). These equations are coupled in space and time on a two-dimensional lattice, which is based on a histological slide of the human prostate peripheral zone (Fig. 1b-d).

We used a histological slide from a normal human prostate to generate a baseline model of the peripheral zone, within which a tumour is initiated. Image segmentation was used to retrieve the basic anatomical glandular structures and cellular densities (Fig. 1b). To reconstruct the tissue domain, histological information was discretized on a two-dimensional lattice (Fig. 1c,d). PCa pathogenesis was simulated by seeding a single abnormal luminal cell inside a duct near the centre of the lattice. Typically, the tumour cell populates the duct through division and then breaches the basement membrane. The tumour mutates and appropriate phenotypes invade throughout the peripheral zone, eventually reaching the edge of the lattice. In our model, as shown in Extended Data Fig. 1, cells migrate to orthogonal positions. Cells are also capable of division and apoptosis, as well as production and consumption of extracellular proteins and growth factors, as dictated to by the cell life cycle flow charts (Fig. 1e).

Many chemokines and cytokines play a documented role in tumour-promoting paracrine interactions[10,11,41,42]. However, the mechanisms of the signalling milieu surrounding tumours are complex and the fine details are not well understood. Dissecting the dialogue between the tumour and the stroma is a major experimental undertaking that would be considerably simplified by the development of integrated mathematical/experimental approaches focusing on cellular consequences rather than individual genes. The cellular phenotype is a product of both genetic and non-genetic determinants and is always defined in relation to a specific context. Cellular selection occurs at the phenotypic level and this is the scale that naturally integrates both intrinsic and extrinsic signals to produce a functional response.

To study the impact of environmental selection on PCa phenotypic heterogeneity, eight initial tumour phenotypes with different levels of growth factor and MMP production were chosen. These are key biological drivers of PCa growth and invasion. Tumour cells in the model mutate randomly (through unbiased drift at division) from their parental phenotype by altering their growth factor and MMP production rates. To explore the role of stroma, two different stromal reactivity phenotypes were modelled: high stromal reactivity (stromal cells that on activation produce high amounts of growth factor) and low stromal reactivity (stromal cells that on activation produce low amounts of growth factor). This leads to 16 different combinations of tumour–stromal growth conditions. We performed a total of 4,800 simulations consisting of 300 repeats for the 16 different tumour–stromal combinations.

Cancer–stroma phenotypic dialogue regulates tumour growth and invasion in a nonlinear manner.

In silico, the level of stromal activation, defined as the proportion of stromal cells activated per year, is significantly correlated with the level of tumour growth (tumour epithelium and reactive stroma). Representations of tumours growing in low and high stromal reactivity are presented (Fig. 2a-d). Tumours, initiated using a single cancer cell that are characterized by low growth factor and MMP production, grow faster in microenvironments with higher stromal reactivity (Fig. 2e). This suggests that the degree of stromal reactivity may be at least as important a driver of differential tumour growth and invasion as the phenotype of the initially seeded tumour cell (Fig. 2f,h). More specifically, tumours grow faster, as measured by time to maximal size, that is, time to the edge of the domain, not only when initiated with an aggressive epithelial phenotype, that is, high levels of growth factor and MMP production, but also when seeded with non-aggressive phenotypes, provided the tumour microenvironment contains high stromal reactivity (Fig. 2f,h,j). These data are consistent with research from our laboratories and others that have emphasized the role of reactive stroma facilitating tumour growth[43].

This model also makes the intriguing prediction that stromal cells with high reactivity can be activated not only within or adjacent to the tumour, but also at some distance beyond the tumour margins (Fig. 2b,g). This phenomenon arises from the growth factor production initiated by the tumour cells, which activates local stromal cells. Once triggered, the paracrine production of growth factor by high stromal reactivity will form an autonomous activation cascade that extends beyond the edge of the tumour (Fig. 2g,i). In the case of low stromal reactivity, reactive stromal cells are only found within the tumour, since they are much more dependent on the growth factor produced by tumour cells directly (Fig. 2a,g). To test the idea of reactive stromal cells inducing further stromal activation, we exposed a benign human prostate fibroblast cell line (BHPrS1) to conditioned medium from either RSG1- or RSG3-derived carcinoma-associated fibroblasts (Fig. 2k). We tested for the expression of three key markers associated with stromal activation (CD90, TGF-β1 and SDF1α) and compared the expression of these in BHPrS1 cells growing in autonomously conditioned medium. Both RSG1-CAF- and RSG3-CAF-conditioned media caused the upregulation of stromal activation markers in this system; no such upregulation was seen with the conditioned medium from benign stromal cells (Fig. 2l).

In summary, differential tumour growth and invasion is correlated with the levels of growth factor production by the initiating tumour cell and the degree of stromal reactivity. However, this is a nonlinear relationship (like Michaelis–Menten kinetics). The results from the in silico model also predict that the degree of stromal reactivity is reflected by the proportion of activated stromal cells. Taken together, this suggests that the phenotypes of the tumour cells and the degree of stromal reactivity could, in combination, act as a more accurate prognostic marker.

Human-derived stroma drives cancer growth in vivo in a stromal grade-specific manner.

To examine the prediction that the nature of reactive stroma plays a role in tumour promotion, we isolated and validated the CAFs from human PCa samples as described

previously[9]. Sections of the source tissues were scored for reactive stromal grade according to standard guidelines (Fig. 3a)[8]. Stromal grading was done without regard to the Gleason score in these samples (Fig. 3b). Analysis of the Ki67 index revealed increased proliferation in cancer cells with RSG3 compared to RSG1 (Fig. 3b) in this model.

Recombinants were generated using an initiated but non-tumorigenic prostate epithelial cell line, BPH1, previously validated as a reporter of the tumour-inducing effects of CAFs[9,10,44]. CAFs alone do not form tumours. In recombinants, CAFs from each RSG group induced tumours in vivo (Fig. 3c). Quantitation of tumour area and invasion revealed that recombinants made using CAFs derived from RSG3 patient tumours were significantly larger and more invasive compared to RSG1-derived cells (Fig. 3d). This demonstrates that stromal characteristics, and especially the extensive stromal response seen in RSG3, can be a powerful driver of tumour growth and local invasion.

To further investigate whether the nature of the epithelium modifies the effects of CAFs, we used three human PCa lines as reporters. Using the same tissue recombination model applied to BPH1 cells, we showed that responses were indeed epithelial cell type-specific. Tumour growth was a function of both the aggressiveness of the epithelial cells and the stromogenic status (RSG1 versus RSG3) of the source of the CAFs. Consistent with in silico model predictions, RSG3-derived CAFs induced significantly larger tumours than RSG1-CAFs in C4-2B (>12-fold) and PC-3 (>six-fold) cells. These lines are both tumorigenic and metastatic when grafted alone, compared to the LNCaP line from which the C4-2B is derived, which result in small tumours when grafted alone. While the recombinants using RSG3-CAFs and LNCaP were slightly larger than their RSG1-derived CAF counterparts, this was a small and statistically non-significant change (Fig. 3e,f). Thus, the response of the epithelial cells seems to be broadly correlated with their degree of aggression, where BPH1 cells alone are non-invasive, as are LNCaP cells, while both PC-3 and C4-2B cells are aggressive and invasive, characteristics that are enhanced by the stromal grade of the source of associated fibroblasts.

Based on the in vitro Ki67 analysis (Fig. 3b), we calculated the percentage of tumour cells undergoing division per year in our in silico model under the two differential stromal conditions and the eight initiating cancer cell phenotypes. Figure 3g shows a consistent increase in the fraction of proliferating tumour cells when using high stromal reactivity, compared to low stromal reactivity. This prediction was further tested in a large cohort of human patient samples. The results show that tumours with RSG3 have a consistently higher proliferation index when analysed for every Gleason category (Gleason scores 6, 7 and 8–10; Fig. 3h). These data support the in vivo data and validate our approach.

An integrated cancer biomarker (ICB): combining RSG and Gleason scoring.

Based on the results obtained in silico and in vivo, we created a clinical combination biomarker with data from the epithelium and stroma. As a stromal marker, we used the percentage of RSG3 within radical prostatectomy PCa, as described previously[17,45-47]. We chose the Gleason score as an epithelial cancer marker. This new ‘ICB’ was tested against biochemical recurrence and PCa-specific death. Optimal cut-off values for the percentage of RSG3 were obtained by using a minimum P value approach[48] for every Gleason category

(Fig. 4a-f). Gleason-score-6 patients with a cut-off of 21% and above reactive stroma (histology shown in Fig. 4a,b); Gleason-score-7 patients with 61% and above reactive stroma (Fig. 4c,d); and Gleason-score-8–10 patients with 71% and above reactive stroma (Fig. 4e,f) were separated.

We used the Cox proportional hazards models to evaluate univariable and multivariable associations of time to death or recurrence with the ICB. The hazard rates of each model were compared to the reference group, namely patients with a Gleason score of 6 and 0–20% of reactive stroma grade RSG3 within the tumour (Table 1). Extra-capsular extension, seminal vesicle invasion, margins, lymph node status and preoperative prostate-specific antigen (PSA) were adjusted in the final multivariable model. Those with Gleason score 6/21–95% of the tumour with RSG3 had a 2.4-fold increased risk for biochemical recurrence (Fig. 4h) and 7.9-fold increased risk of PCa-specific death (Fig. 4g) than baseline. In the Gleason-score-7 category, those with 0–60% of the tumour with RSG3 had a 3.2- and 5.6-fold risk of biochemical recurrence (Fig. 4j) and PCa-specific death (Fig. 4i), while those with >61% had a 4.3- and 12.7-fold risk of biochemical recurrence (Fig. 4j) and PCa-specific death, respectively (Fig. 4i). Even within the Gleason-score-8–10 categories, those with 0–70% of the tumour with RSG3 had a 3.2- and 18.6-fold risk of biochemical recurrence (Fig. 4l) and PCa-specific death (Fig. 4k), while those with >71% had a 7.3- and 56-fold risk of biochemical recurrence and PCa-specific death, respectively (Fig. 4l,k). Note the difference that the increased RSG has on the hazard ratios in every category; these were highly significant ($P < 0.0001$; Table 1).

To validate the results of the survival analyses, we looked at the performance of the new ICB against current standard-of-care predictive models by conducting logistic regression models where the binary outcome of biochemical recurrence or death was examined. We evaluated the Akaike information criterion (AIC) to conduct predictive model comparisons as a measure of the relative quality of the statistical models, as well as controlling for both goodness of fit and the complexity of the model. Given a set of candidate models for the data, the preferred model is the one with the minimum AIC value. The ICB has a significantly lower AIC than the Gleason and RSG3 alone, both for biochemical recurrence (713.15 « 1016.69) and PCa-specific death (258.33 « 418.25) (Fig. 4m). The same is true when incorporating the current clinico-pathological parameters (seminal vesicle invasion, Union for International Cancer Control staging, extra-capsular extension, margins) into the model. The AIC for the model with the ICB is much lower than the Gleason score with the current clinico-pathological parameters, both for biochemical recurrence (552.95 « 702.63) and PCa-specific death (233.7 « 308.17) (Fig. 4n). The addition of the ICB significantly helps the model specification. This demonstrates that the interaction between Gleason score and stromal grading provides more information than either marker alone in the model.

Reactive stroma drives cancer evolution and heterogeneity.

To better understand how the dialogue between tumour cells and stromal reactivity drives evolution in our mathematical representation, we examined two conditions of stromal reactivity (Fig. 5a-e). When a non-aggressive tumour cell (that is, one with low rates of growth factor and MMP production) is seeded in our multiscale prostate peripheral

zone model with low stromal reactivity, the rate of tumour evolution is faster than in a high stromal reactivity environment (Fig. 5f). Interestingly this does not translate into a larger tumour since the competition between tissues (tumour and stroma) for the limited growth factor resource slows overall growth (Fig. 5a-e). However; this competition places a strong selection pressure on the tumour, driving it towards cell phenotypes that produce more growth factor to survive. The increased selection pressure varies both spatially and temporally, depending on the relative local abundance of tumour and stromal cells. The resulting tumours tend to be more phenotypically heterogeneous (Fig. 5c). Conversely, the selection pressure for more aggressive phenotypes is much lower in tumour microenvironments characterized by high stromal reactivity, even when the initial tumour cell is not aggressive (Fig. 5e). The resulting tumours are less phenotypically heterogeneous and more driven by drift than selection. These tumours are the ones that grow and invade the fastest. This phenomenon is due to the abundance of stromal-derived growth factor not only within the tumour, but also further afield because of extended stromal activation. Of note is that the other evolving trait, MMP production, does not seem to be differentially selected between the high and low stromal reactivity microenvironments (Extended Data Fig. 2). However, there is a trend for higher production in the high stromal reactivity microenvironment, which may be due to the more rapid growth these tumours display.

An intriguing prediction of our model is that the differences in tumour evolution are modulated in a nonlinear way by the aggressiveness of the initiating phenotype (Fig. 5f). In the mid-range of initiating cell phenotypes (25–35), the difference in tumour evolution rates between high and low reactive stroma is greatest (Fig. 5f), whereas the difference is minimized for the least and most aggressive initiating phenotypes (10 and 60, respectively). This is reminiscent of our previous findings where RSG3 had better predictive ability in tumours with a Gleason score of 7, compared to 8–10 (ref. [15]).

To test this prediction in human samples, we performed an analysis of three well-established PCa molecular regulators: androgen receptor; phosphorylated Akt1; and activated nuclear factor kappa B (NF-κB, phospho-p65). The analysis was performed on triple-immunostained tissue sections of a large cohort of patients, described previously[8], using image deconvolution, tissue compartment segmentation (that is, tumour versus stroma) and cell-by-cell analysis of each marker. Figure 5g-l shows the tissue examples from patients with RSG1 (Fig. 5g-i) versus RSG3 (Fig. 5j-l), where cell colour reflects the expression intensity for each of the individual cell expression of phosphorylated Akt, androgen receptor and the central immune regulator NF-κB.

Further analysis was performed on tissues from each Gleason score category, and over RSG1 (Fig. 5m-o, blue) and RSG3 (Fig. 5m-o, red), like the ICB and in silico model predictions. We quantified Akt, androgen receptor and NF-κB across all individual cells in tissues from a large population of patients (Fig. 5m-o). Results of the average expression across all cells show a trend towards selection of a more aggressive phenotype in low reactive stroma (that is, high levels of biomarker expression; see Extended Data Fig. 3). To isolate a subset of the tumour cell population that would be under greater selection pressure, we analysed the top 1% of expressing cells in each of the selected patients (Fig. 5m-o). We identified a statistically significant difference between patients with RSG1 and RSG3,

with higher expression of androgen receptor and Akt in RSG1, than in RSG3, in this cell population. Therefore, low reactive stroma (RSG1) appears to be associated with increased expression of Akt and androgen receptor (compared to high reactive stroma, RSG3) and this effect is more pronounced in Gleason-score-6 and −7 tumours. The in silico predictions (Fig. 5f) show that intermediate tumour cell phenotypes evolve towards higher growth factor production under low stromal reactivity conditions, showing a similar trend to these patient samples.

We performed co-culture experiments using three human prostate cell lines (LNCaP, C4-2B and PC-3) representing mildly, moderately and aggressively invasive disease in medium conditioned by RSG1 or RSG3 tumour-derived fibroblasts (Fig. 5p-r). Equal numbers of cells, either as pairs or all three lines together, were plated and the number of each cell type at the end of the culture period was counted (Extended Data Fig. 4). These studies were consistent with the mathematical predictions in that the most aggressive cell type did not outgrow the other populations; in most situations where all three lines were co-cultured, the dominant cell at the end of the study was the intermediate C4-2B cell line (Fig. 5q).

On inspection of some of the patient samples, we noticed significant gradients in Akt and androgen receptor expression. We reasoned that such gradients may be indicative of an evolving population. We developed a simple algorithm to examine the slope of expression across the triple-stained samples by analysing the change in expression spatially across each individual sample (Fig. 5v); the larger the slope the more quickly expression changes with distance. We observed the largest slopes in Gleason-score-7 patients with RSG1 for all three markers (Akt, androgen receptor and NF-κB; Fig. 5s-u). If we view the slope as a metric for evolution, this is again consistent with our in silico predictions that the greatest evolution occurs at intermediate phenotypes with low stromal reactivity (see Fig. 5f).

Discussion

In vitro and in vivo methods constitute the backbone of current biological knowledge. Yet, they are limited in their ability to model complex interactions and diverse dynamics because of their reductionist nature. Mathematical modelling readily captures the complex nature of cancer pathogenesis, both spatially and temporally. Critically, these models allow us to manipulate multiple factors both in isolation and simultaneously, combining key features as well as teasing apart their individual contributions, while still predicting how their interactions will shape tumour behaviour. Features such as interactions at different scales and the stochastic nature of evolution can be tested experimentally in silico. Therefore, to better understand the dialogue between tumour and stroma, we have implemented a hybrid multiscale model of carcinogenesis in the prostate peripheral zone. Results from this model generated insights into the role of stroma in cancer evolution and led us to new ideas. Our model generated multiple hypotheses, some of which were tested in vitro and in vivo and subsequently validated in a large cohort of patients. This integrated paradigm merges data from biology and pathology on the microenvironmental regulation of PCa cell behaviour and leads to insights in understanding cancer evolution, heterogeneity and progression. Our theoretical framework is a significant step in the development of mathematical models that better mimic human PCa.

Interactions between tumour stroma and epithelium are established regulators of PCa progression[9,49,50]. Cells derived from the reactive stroma (CAFs) can drive tumour growth and invasion[10,44]. In PCa, the degree of stromogenic response to a tumour correlates to biochemical progression and cancer-specific death[8,17]. Our multiscale prostate peripheral zone model recapitulates these observations, demonstrating its ability to reproduce known biological and pathological processes and building confidence in its predictive power.

Stroma plays an important role in the development of PCa. Our model goes beyond this finding and predicts that the interplay between stroma and epithelium (that is, the balance of individual cancer cell aggressiveness and stromal reactivity) is more important than either stromal or epithelial properties alone. From our model, we have derived the following predictions: (1) the balance between stromal activation and tumour aggressiveness is key to tumour progression; (2) stromal cells can enhance stromal activation, suggesting that reactive stroma can become self-activating under certain conditions; and (3) the degree of stromal reactivity regulates tumour epithelial evolution. Our integrated approach allowed us to test and validate hypotheses 1 and 2, and provide strong support for hypothesis 3.

The model predicts that growth factors produced by either the reactive stroma or cancer cells play complimentary roles and may compensate for each other. Specifically, to our knowledge, the idea that reactive stroma may contribute to further stromal activation is new. The underlying mechanisms of this phenomenon are under investigation and await a more complete description of the tumour stroma phenotype from PCa patients on a single-cell basis. The significance of this balance was validated using both in vivo modelling and human studies. Results in both mice and humans were consistent with our mathematical prediction.

Concordantly, we identified that Gleason score and RSG quantitation (stromogenic carcinoma), when combined as the ICB, improve predictive power. In fact, RSG quantitation significantly stratifies all the recurrence and death risk categories as suggested by the current Gleason grading system. Due to its combinatorial nature, this system better addresses the issue of heterogeneity in both cancer differentiation and degree of stromal response. These results suggest that for patients whose tissue shows a high percentage of the tumour with stromogenic response, the risk should be considered higher than the standard Gleason assessment. Conversely, low percentage of RSG3 in a patient’s biopsy would imply a lower risk than the standard Gleason assessment. We showed that the degree of stromal reactivity, when integrated with the current clinical in use methodology (Gleason score with clinico-pathological parameters), significantly improves PCa prognosis and may be useful to modify the way patients are treated. We stress that the ICB can stratify most of the problematic intermediate Gleason-score-7 category. It is also important to note that the percentage of tumour with RSG3 varies between Gleason subgroups. Gleason score 6 requires a minimum of 21% of the tumour with RSG3 to be predictive. This increases to 61 and 71% in Gleason score 7 and Gleason score 8–10, respectively, demonstrating that the dynamic of the interplay between stroma and cancer has differential thresholds. This supports the balance concept between stroma and cancer cells identified in the mathematical model.

The most important prediction of this study is that evolutionary dynamics in tumours growing in the presence of stroma with high stromal reactivity is different from those growing in association with low stromal reactivity. The clear implication of this finding is that the progression of tumours reflects the ability of the host to respond to specific stimuli. In low stromal reactivity situations, the rate of epithelial cell evolution is higher, leading to increased heterogeneity with selection for increased growth factor production. In contrast, high stromal reactivity results in lower evolutionary pressures on the tumour epithelium, since enough growth factor is provided by the reactive stromal cells. Therefore, the differentiation state of cancer cells tends to drift in terms of growth factor production, rather than undergoing rigorous selection for the high expression needed for survival when an outside source is unavailable. This suggests that high levels of stromally produced growth factor may result in less aggressive individual cancer cell phenotypes; nonetheless, the tumour constitutes a larger invasive mass. Using cell-by-cell data analysis of triple-immunostained biomarkers in a cohort of human patients, we identified a signal that indicated that PCa cells growing with low reactive stroma (RSG1) have a higher rate of selection, leading to evolution of a more advanced phenotype. These changes were more significant in Gleason-score-6 and −7 patients, than Gleason score 8–10, (Fig. 5g), which is concordant with our mathematical model predictions that identify greater evolution when starting with intermediate cancer cell phenotypes (Fig. 5e). This makes sense from an evolutionary perspective, since more aggressive tumours (that is, Gleason score 8–10) may be less dependent on stroma for supplying growth factor, or they may require higher levels of stromal involvement to make a survival difference.

These evolutionary dynamics and associated tumour heterogeneity demonstrate why it is not possible to accurately assess patient risk by relying exclusively on tumour cell features (tissue architecture and molecular markers of individual cancer cells), especially for tumours with intermediate grades, which are, typically, the more challenging ones to assess.

Therefore, our results suggest two broad mechanisms that lead to invasive tumour growth. In the first case, the presence of highly reactive stroma within and surrounding the tumour provides excess growth factor, fuelling growth. A positive feedback loop leads to a self-activating reactive stromal compartment, allowing tumour growth to continue indefinitely. This first case would correspond to high RSG and intermediate Gleason scores. In the second case, a lack of stromal reactivity instead promotes the evolution of tumour cell phenotypes favouring growth factor production. These altered cells, by nature, are less stromally dependent and eventually form invasive tumours. However, the tumour is relatively indolent until these growth factor-producing cells have developed and been selected, which could take time (perhaps even beyond the lifetime of the patient) when compared to the first case, where a tumour can immediately access high levels of growth factor.

In conclusion, our data indicate that the interactions between tumour cells and reactive stroma shape the evolutionary dynamics of PCa and explain overall tumour aggressiveness (Fig. 6). We show that the degree of stromal reactivity, when coupled with the current clinical biomarkers, significantly improves PCa prognosis, both for death and recurrence, that may alter treatment decisions. We also show that stromal reactivity correlates directly

with tumour growth but inversely modulates tumour evolution. This lends weight to the idea that aggressive, stromal-independent PCa may be an inevitable evolutionary result of poor stromal reactivity and that purely tumour-centric metrics of aggressiveness may be insufficient in terms of clinical outcome.

Methods

Multiscale prostate peripheral zone model.

The model we developed builds on the HCA model described by Basanta[28] and Anderson[39]. The definition of an HCA model requires a set of partial differential equations that characterize the physical microenvironment, a set of life-cycle flow charts that characterize the behaviour of the cells under microenvironmental constraints (Fig. 1e) and a cellular automaton framework to integrate them. The following system of nonlinear partial differential equations define growth factor (G), MMP (E) and ECM/basement membrane (M) as the three key continuous microenvironmental variables:

$$\overbrace{\frac{\partial G(x,y,t)}{\partial t}}^{\text{Growth factor dynamics}} = \overbrace{\nabla(\delta_G(m_0 - M)\nabla G)}^{\text{Diffusion-mediated by basement membrane}} + \overbrace{\alpha_B \tilde{B}}^{\text{Basal cell production}} + \overbrace{\gamma \tilde{C}}^{\text{Tumor cell production}} + \overbrace{\chi_{\mathrm{RS}}\mathrm{RSG}}^{\text{Reactive stromal cell production}} - \overbrace{\rho_{\mathrm{RS}}\mathrm{RSG}}^{\text{Reactive stromal cell consumption}} - \overbrace{\beta_{\mathrm{S}}\mathrm{SG}}^{\text{Stromal cell consumption}} - \overbrace{\mu_E \mathrm{MG}}^{\text{Binding by ECM/basal membrane}} - \overbrace{\eta_{\mathrm{L}}\mathrm{LG}}^{\text{Luminal cell consumption}} - \overbrace{\varphi G}^{\text{Natural decay}}$$

$$\overbrace{\frac{\partial E(x,y,t)}{\partial t}}^{\text{MMP dynamics}} = \overbrace{\delta_E \nabla^2 E}^{\text{Enzyme diffusion}} + \overbrace{\zeta \tilde{C}}^{\text{Tumor cell production}} - \overbrace{\kappa \mathrm{ME}}^{\text{Enzyme degradation}}$$

$$\overbrace{\frac{\partial M(x,y,t)}{\partial t}}^{\text{ECM/basal membrane dynamics}} = \overbrace{\nu_B \tilde{B}}^{\text{Basal cell production}} + \overbrace{\tau_{\mathrm{I}}\mathrm{IG}}^{\text{Inflammatory cells facilitating production}} - \overbrace{\sigma \mathrm{ME}}^{\text{Enzymatic-ECM / basal membrane degradation}} \quad (1)$$

δ_G and δ_E are the growth factor and MMP diffusion coefficients, respectively; x,y represents the x and y dimensions of the two-dimensional domain; t is time; m_0, α_B, γ, χ_{RS}, ρ_{RS}, β_{S}, μ_E, η_{L}, φ, ζ, κ, ν_B, τ_{I} and σ are positive constants with biologically significant values as based on Basanta[28]. Then, a discretized form of these equations is solved numerically on a two-dimensional lattice that represents a small slice of prostate tissue. All cell types (tumour, basal, luminal, stromal and inflammatory) are modulated by the microenvironment on this lattice and can migrate, proliferate, die and mutate according to the life-cycle flow charts (Fig. 1e). Further detail can be found in the Supplementary Information and Extended Data Fig. 1.

Tumour cells in the model have two continuously variable phenotypes, namely growth factor (γ) and MMP (ζ) production. These traits are passed from a parent tumour cell to its two daughter cells with some small variation, chosen at random from an interval equally weighted in both directions to avoid biased drift. The model is agnostic with respect to specific biological mechanisms that underlie this drift, which could include gradual accumulation of mutations, regulation of gene transcription by epigenetics or aneuploidy, or changes in the number or structure of organelles, for example. The evolution of these phenotypes in time and space is an important consideration of this work.

The switch between stroma (S) and reactive stroma (RS) phenotypes is driven by the growth factor stimulus. Reactive stromal cells are activated if the level of growth factor (G) is above the threshold G_{RS} and are deactivated if the growth factor level G falls below the threshold G_{RS}.

Clinical specimens.

To validate the findings of the mathematical model and its biological validation, we used a unique human tissue resource. The cohort was selected from patients operated on by a single surgeon, without additional forms of therapy other than surgery, and over 20 years of follow-up.

Cohort enrolment and follow-up.

The Baylor College of Medicine Prostate Cancer database contains information for over 9,000 patients who underwent radical prostatectomies at one of the College's affiliated institutions and provided tissues (institutional review board no. H-1158). Of these patients, 1,291 were operated on by a single surgeon between 1983 and 1998 without any previous form of adjuvant therapy, such as radiation or hormonal therapy. This study was approved by the Baylor College of Medicine institutional review board (no. H-11436).

Radical prostatectomy specimens from these patients were processed using whole-mount slides according to procedures described previously[51]. After surgery, the prostate specimens were sliced into 5-mm-thick tissue whole mounts. The tissue slices were then fixed in 10% neutral buffered formalin and embedded in paraffin according to a routine procedure. A single pathologist performed the pathological analysis, which included staging, pathological staging, margins, capsular penetration, seminal vesicle invasion, primary and secondary Gleason grades from biopsy and prostatectomy, lymph node status, tumour volume and geographical location. The clinical and pathological data of patients who met the entry criteria were available for analysis. The clinical follow-up data include PSA recurrence (defined as a PSA of 0.4 ng or two consecutive rises), clinical metastasis and PCa-specific death.

Clinical characteristics.

The age of patients ranged from 37 to 80 with a mean of 62 and median of 63 years. Patients were followed post-operatively for an average of 42.08 (mean) and 33.2 months (s.d.), a median of 45.2 months and a maximum of 167.74 months. Preoperative PSA level was available in 603 PCa cases and ranged from 0.3 to 100 ng ml^{-1} with a median of 7.2 ng

ml^{-1} and an s.d. of 10.99 ng ml^{-1}. Approximately 30% of patients had a preoperative PSA level of 10.5 ng ml^{-1}. Approximately 44.6% had a Gleason score of 6; 48.6% had a Gleason score of 6 or 7; and 6.8% had a higher Gleason score (8–10). Lymph node metastasis was found in 40 (6.4%) patients and biochemical recurrence was seen in 120 patients (19.3%). Extra-capsular extension was found in 44.5%. Margins were positive in 15.3% and seminal vesicle invasion had occurred in 12.4% of patients. For this study, we quantified the area of stromogenic carcinoma pattern (RSG) tumour with high risk in the whole-mount-embedded radical prostatectomy specimens in a percentile fashion[17].

Statistical analysis.

Cox proportional hazards regression analyses for each of biochemical recurrence and PCa-specific death were conducted to evaluate univariable and multivariable associations between a stromal marker (that is, the percentage of RSG3 within radical prostatectomy PCa) and risk of recurrence or death. Important standard clinico-pathological risk factors such as Gleason score, extra-capsular extension, seminal vesicle invasion, margins, lymph node status and preoperative PSA were also considered while developing multivariable models to examine the contribution of a stromal marker (that is, percentage RSG3) over traditional factors. Specifically, we focused on determining the effect of stromal marker addition on epithelial cancer marker (that is, Gleason score) by evaluating whether the association between Gleason score and risk of recurrence (or death) differs by levels of percentage RSG3. This led to combining these two markers, resulting in the ICB. While developing the integrated marker, assessment of linearity/functional form and residuals[52] was made to ensure that the underlying linearity assumptions between the predictors and outcome were valid. To establish optimal cut-off values of percentage RSG3 for every Gleason score category, we used a minimum *P* value approach as well as goodness-of-fit tests for overall significance of the model[53]. A test of proportional hazards assumption was also performed and indicated that there was no statistically significant evidence of assumption violation[52,54].

To validate our findings from the survival analyses, we looked at the predictive performance of the new ICB against current standard clinico-pathological risk factors by conducting multivariable logistic regression models, where the binary outcome of biochemical recurrence or death was examined. The prediction accuracy of each model was measured using the area under the receiver operating characteristic area under the curve (AUC).

Given the fact that the increase in AUC was very small when the model already includes highly significant standard risk factors (for example, AUC > 0.85), the magnitude of improvement in AUC may not be nearly as meaningful as the value of the AUC itself[55]. Therefore, in addition to the AUC, we considered deviance-based measures such as the AIC, which is widely used to examine whether the addition of an extra independent variable improves the model specification (that is, the relative quality of the model), while controlling for goodness of fit and the complexity of the model at the same time. The Hosmer–Lemeshow goodness-of-fit test was also constructed to examine the agreement between observed outcomes and predictions. For the statistical analysis, we used measurements that were taken from distinct samples. All analyses were performed primarily

using widely available tools in SAS v.9.4 (SAS Institute). All tests were two-sided at a significance level of 0.05.

Androgen receptor, pAkt and pNF-κB p65 (phospho S276) triple staining.

New tissue microarray slides were triple immunohistochemically stained by using the androgen receptor (catalogue no. CM109A; Biocare Medical), pAkt (catalogue no. M3628; Dako) and pNF-κB p65 (phospho S276) (catalogue no. ab106129; Abcam) antibodies. Before the triple staining, all three antibodies were tested in test tissue microarray slides containing different human prostate tissue samples. Briefly, sections were deparaffinized in xylene, rehydrated through decreasing concentrations of alcohol ending in PBS, subjected to heat-induced antigen retrieval in Target Retrieval Solution (pH 9.0, catalogue no. S2367; Dako) for 4 min at 125 °C in a Pascal instrument (catalogue no. S280030; Dako) and allowed to cool off at room temperature. Endogenous peroxidase activity was quenched in 3% hydrogen peroxide solution in distilled water for 10 min at room temperature. To inhibit non-specific staining, sections were incubated with a protein blocking solution (catalogue no. X0909; Dako) for 10 min at room temperature, then incubated with a mixture of mouse monoclonal antibody against androgen receptor (1:100) and rabbit polyclonal antibody against pAkt (1:10) in antibody diluent (catalogue no. S0809; Dako) for 1 h at room temperature. Sections were washed and the bound antibodies were detected using the MACH2 Double Stain 2 Polymer Detection kit (mouse-HRP + rabbit-AP, catalogue no. MRCT525; Biocare Medical), with 3,3'-diaminobenzidine (for androgen receptor) and Vulcan Fast Red (for Akt, catalogue no. FR805; Biocare Medical) as chromogens.

To ensure that the third antibody staining would not cross-react with the androgen receptor and pAkt staining, sections were incubated with a denaturing solution for 2 min (catalogue no. DNS001; Biocare Medical), then incubated with rabbit polyclonal antibody against pNF-κB p65 (phospho S276) (1:300) for 2 h at room temperature. Sections were washed and the bound antibody was detected using a MACH2 Rabbit HRP-Polymer (catalogue no. RHRP520; Biocare Medical) with Vina Green (catalogue no. BRR807AH; Biocare Medical) as chromogen.

Finally, sections were counterstained with CAT haematoxylin (1:4 diluted with water for 40 s, catalogue no. CATHE; Biocare Medical) and bluing reagent (10 s, catalogue no. SL203; Statlab Medical Products), then air-dried at 65 °C for 15 min and mounted with EcoMount (catalogue no. EM897L; Biocare Medical).

Quantification of androgen receptor, pAkt and pNF-κ p65 using image deconvolution, segmentation and analysis.

Hot spot areas of expression of the 3 biomarkers within the PCa tissues were imaged using the Vectra v.1.4.0 (one 200× images per core). A combination of deconvolution imaging (such as Vectra) and image segmentation technology (such as InForm v.2.1.1) was used.

All immunostained slides were digitized with the use of a multispectral imaging system that enabled capturing a series of images from a single field at a spectrum of specific wavelengths (420–720 nm). Multiple series of images taken at different wavelengths at one shut is called 'image cube'. Image cubes were created for every case and saved in both

multispectral .im3 and JPEG formats. All images were taken at 200× magnification and captured >95% of 0.6 mm tissue cores. The measurement of image spectral wavelengths enables more accurate separation of tissue and cellular components.

The InForm image segmentation system was used to separate non-neoplastic and neoplastic PCa tissues from the normal muscular host stromal tissues, as well as reactive stroma. The signal was analysed only in the epithelial component.

Image segmentation software was used for tissue and cellular analysis of the tumoural stroma in the prostatic adenocarcinoma. Pictures from each case were reviewed individually; only tumour and tumoural stroma areas were selected for further analysis.

Tissues were algorithm-segmented into compartments (cancer epithelium and cancer stroma); each compartment was segmented into individual cells and each cell was segmented into nuclei and cytoplasm. Individual cells were recognized within each compartment and the androgen receptor, pAkt and pNF-κB p65 signal was separated and analysed in each compartment of the tumour separately in each individual cell. All were analysed in the cytoplasm of the cancer cells. In conclusion, we provided read-outs per individual cells, in each compartment, each with coordinates for spatial localization within the tissues.

Isolation and characterization of CAFs.

Isolation and validation of the tumour-inducing abilities of CAFs from tissue samples was performed as described previously[9]. After enzymatic (collagenase) digestion of prostate tissues, cells were enriched for fibroblasts by sub-culturing (up to 4 passages) in 10% Roswell Park Memorial Institute (RPMI) medium[9]. Characterization of fibroblasts included the assessment of stromal markers (smooth muscle actin and vimentin) and lack of epithelial contamination (wide-spectrum cytokeratin) by western blot analysis. Stromogenic (or RSG) classification of 6 CAF strains isolated from patients (3 from RSG1 and 3 from RSG3) was performed by scoring of Masson's trichrome-stained tissues according to standard guidelines[8]. The RSG grading system is based on the percentage of intratumour reactive stroma (stained for collagen by Masson's trichrome staining) where RSG0 = <5%, RSG1 = 5–15%, RSG2 = 15–50% and RSG4 = >50%. Concurrently, samples were scored for Gleason grade. The Gleason score of the CAFs used in the in vitro/in vivo studies from RSG1 tumours were 6 (3 + 3), 7 (3 + 4) and 7 (4 + 3); in RSG3 tumours, they were 7 (4 + 3), 7 (4 + 3) and 7 (3 + 4). Immunohistochemical staining for Ki67 was performed and a labelling index calculated for each sample.

Effects of RSG status of source material on the tumour-inducing capability of CAF cells.

To test the effects of RSG characteristics on tumour growth, an initiated but non-tumorigenic prostate epithelial cell line BPH1 (100k) was recombined with CAFs (250k) with different RSGs and grafted under the renal capsule of castrated, testosterone-supplemented CB17Icr/Hsd-severe combined immunodeficient mice (SCID; Harlan) as described previously[44]. The BPH1 cell line responds to the pro-tumorigenic effects of CAFs by undergoing malignant transformation[9]. We had previously noted that the volume of such tumours varies according to the patient source of CAFs but had not examined this phenomenon formally. CAFs from each RSG group were used in a standardized recombination assay and grafted to SCID mice

for 12 weeks. The resultant tumours were collected; their area in a central cross-section and invasiveness measured from the surface of the kidney to the deepest point of penetration was determined.

To test how PCa cell lines respond to CAFs, and specifically to determine whether such a response is a function of the source tumour from which the CAFs were derived, three cell lines (100k LNCaP, C4-2B and PC-3) representing progressively increasingly aggressive disease were combined with CAFs (250k) from various RSG-defined tumours and tested in tissue recombination experiments in SCID mice, as described earlier.

Cell culture conditions.

The stromal cell lines BHPrS1 (our stocks), primary normal prostate fibroblasts (NPF) and CAFs derived from RSG1 and RSG3 tumours were grown in 5% FCS RPMI 1640 medium[9,10]. The non-tumorigenic prostate epithelial cell line BPH1 was cultured in 5% RPMI medium. The PCa epithelial cell line LNCaP and its derivative C4-2B (from the CCL Core at the MD Anderson Center) were cultured in T medium (10% FCS DMEM/F12 culture medium) plus supplements[56]. PC-3 cells (ATCC CRL-1435) were cultured in F-12K medium.

Effects of stroma-conditioned medium on growth.

The NPFs and CAFs derived from RSG1 and RSG3 tumours were grown in RPMI 1640 supplemented with 0.5% FCS and 10^{-8} M testosterone for 48–72 h, after which the media were collected, centrifuged and filtered (0.45 μm).

PC-3, C4-2B and LNCaP cells (from ATCC and the MD Anderson Center) representing progressively less aggressive tumours, were transduced with lentiviral constructs carrying fluorescent colour tags (colours were a gift from A. Zjilstra). Cells were grown under positive blasticidin selection; then, moderate colour expression was selected using fluorescence-activated cell sorting to generate green, red and blue lines designated as PC-3-GFP, LNCaP-BFP and C4-2B-RFP. Cells were seeded (all combination mixtures of single-cell line alone, three pair combinations and all three colours together) in 96-well dishes in triplicate at an initial density of 5,000 total cells per well. The cells were allowed 24 h to attach after which the medium was changed to a 1:1 mixture of CAF-CM and RPMI 1640, serum-adjusted to 0.5% FCS. Medium was changed twice weekly for 4 weeks; images were taken at the end of each week to determine cell distribution. At the end of the experiment, cells were passed through a MACSQuant Analyzer (Miltenyi Biotec) to generate colour-specific counts of total cells per well.

Extended Data

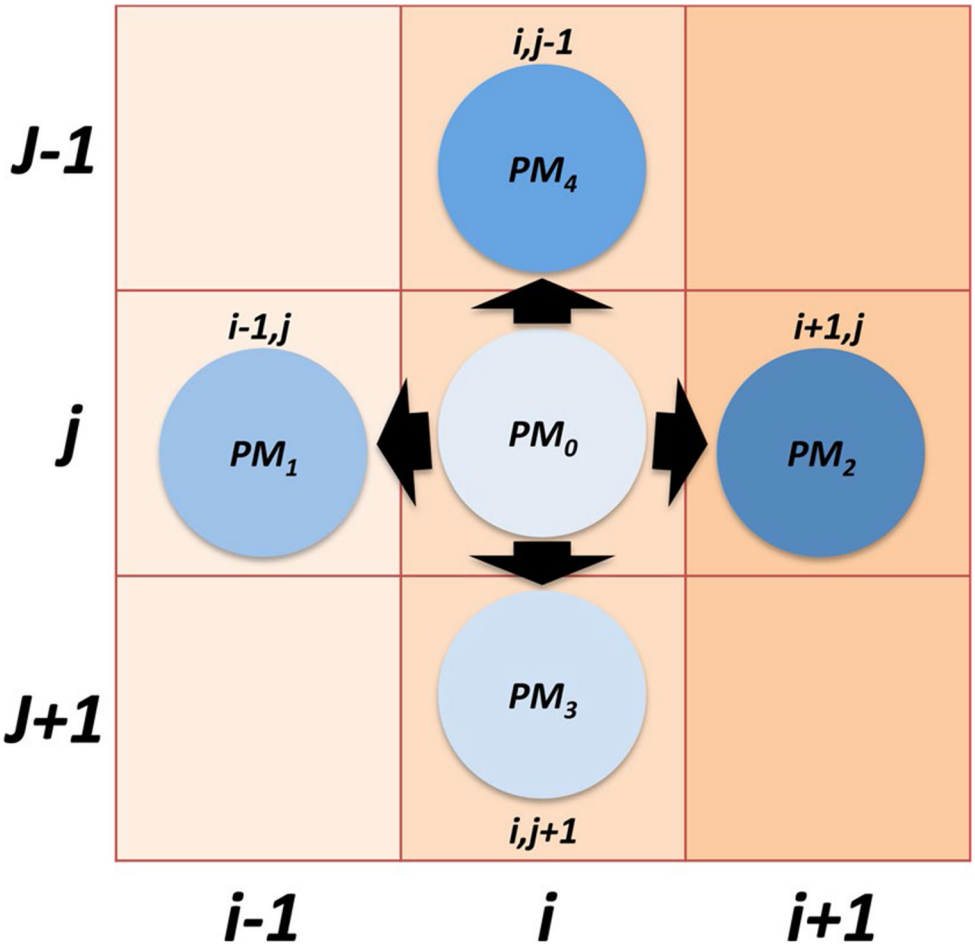

Extended Data Fig. 1 |. Representation of movement probabilities.
Representation of the probabilities of cell located at coordinates (*i,j*) moving to one of its four orthogonal neighbors ($PM_{1\text{-}4}$) or remaining stationary (PM_0).

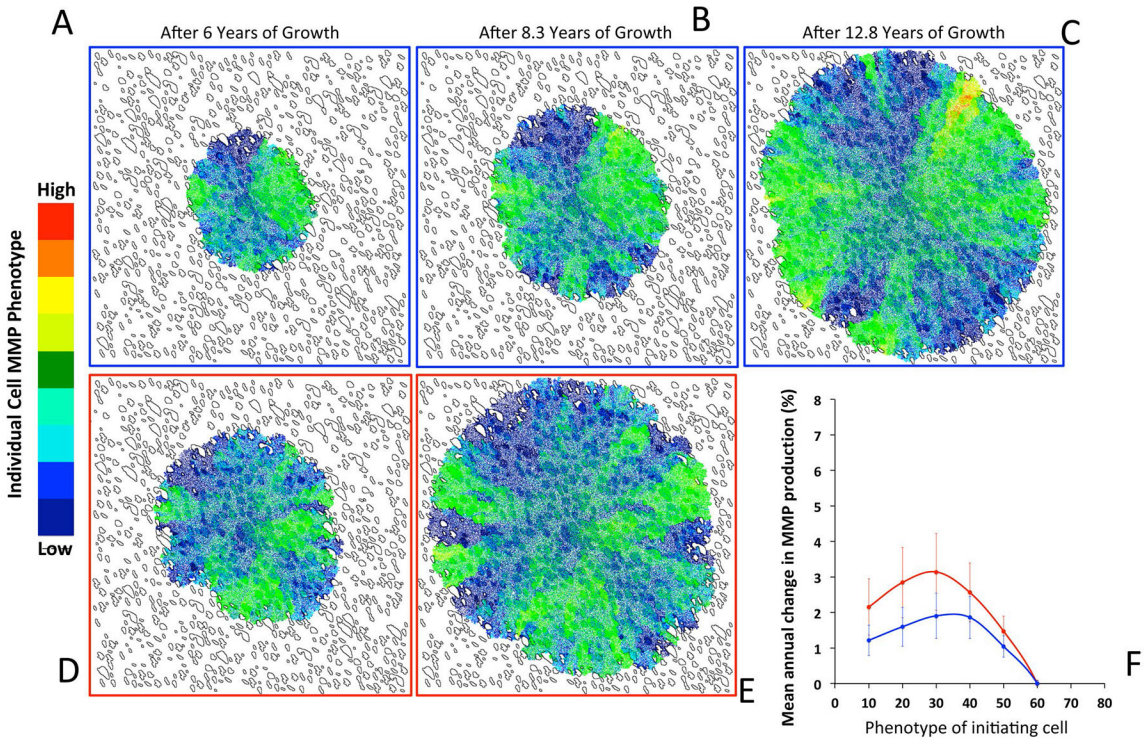

Extended Data Fig. 2 |. Evolution of tumour cell MMP production under low and high SR conditions.

The evolution of tumour cell phenotypes through space and time (6-12.8 years) under low (blue) and high (red) SR conditions (this is the MMP equivalent of Fig. 5a-f). Heat map shows tumour cell phenotype (MMP production) distribution in low SR (**a-c**) and high SR (**d, e**). Tumor cell phenotypic change in MMP production from 8 different initiating phenotypes in high (red) and low (blue) SR environments (the average change and standard deviation across 100 simulations per initiating phenotype) is show in panel **f**.

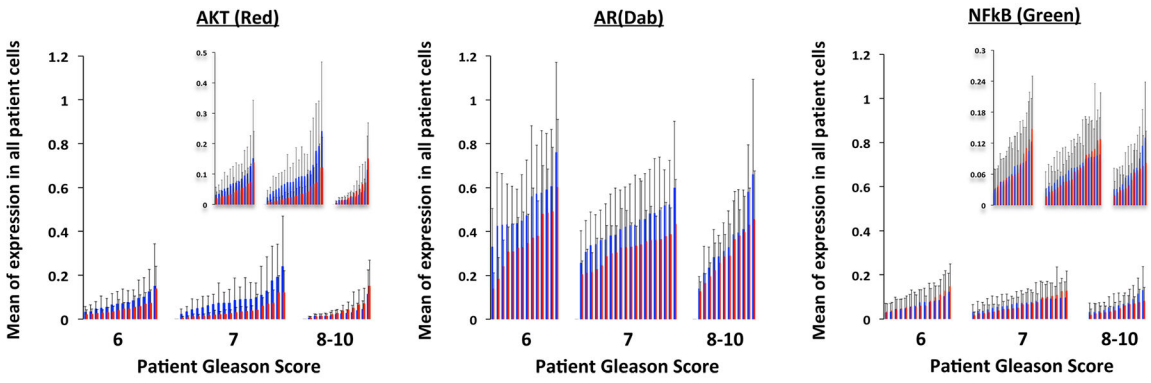

Extended Data Fig. 3 |. SR drives tumour cell evolution and progression.

Extension of Fig. 5m-o. Single cell quantitative analysis of the triple immunostained (AKT, AR and NFkB) tissue sections for patients with RSG1 (blue) vs. RSG3 (red) in each Gleason category. Expression in all cells from each of the patient's biopsies are shown, each

individual bar represents the average (and deviation) for a single patient over all cells. Insets for AKT and NFkB have more appropriate y-axis scales to better illustrate differences.

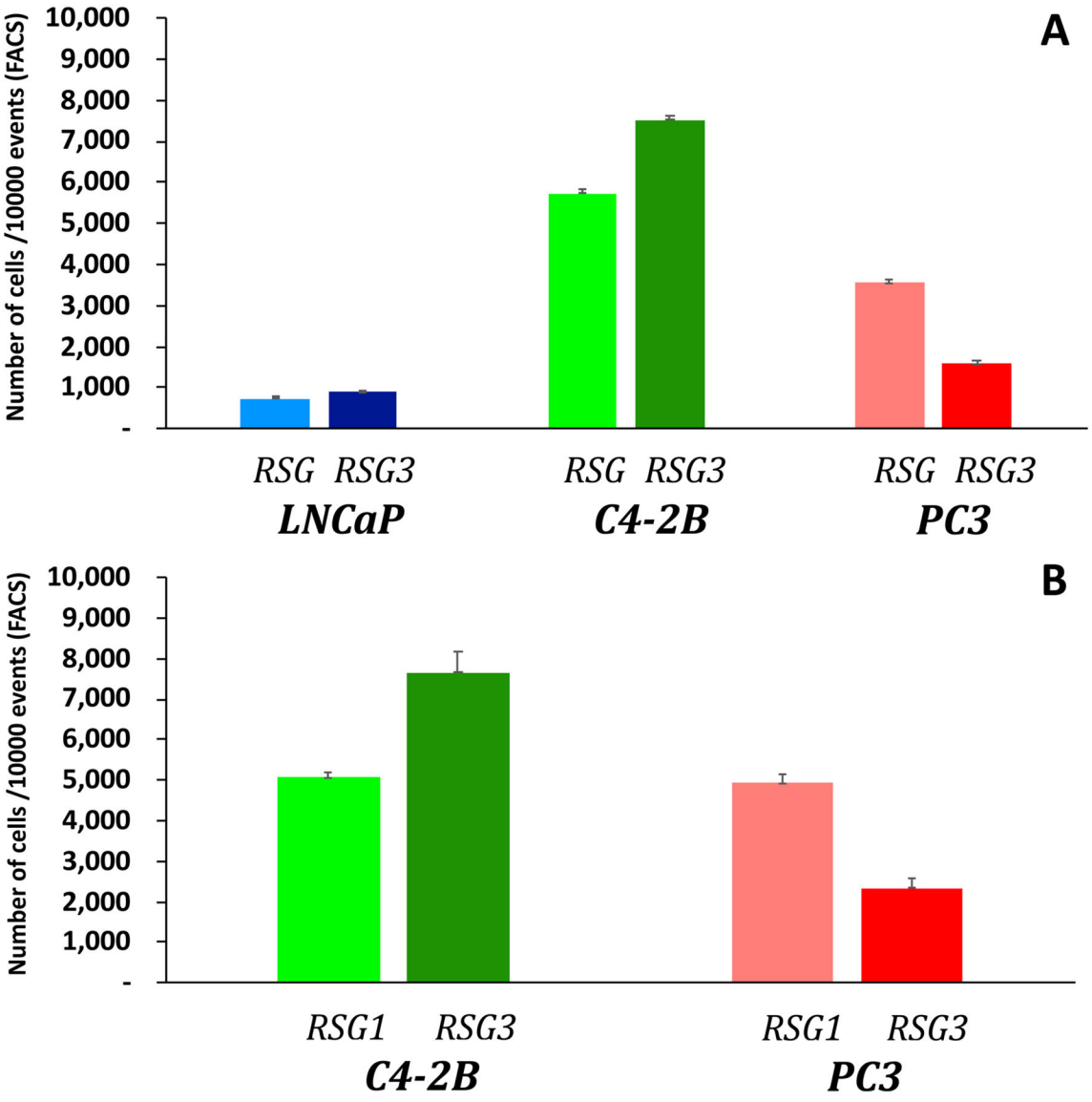

Extended Data Fig. 4 |. Co-culture experiment details (Relevant to Fig. 5q, r).

a. Prostate Cancer cell lines LNCaP-BFP, C4-2B-RFP and PC3-GFP were cultured in the presence of conditioned medium (CM) from RSG1-CAF or RSG3-CAF for 4 weeks. Quantitation of individual cell populations was determined by FACS analysis. The number of each cell line out of 10,000 gated total number of cells (Y-axis) is shown for each cell line. **b**. Co-culture experiments using aggressive C4-2B and PC3 cells exposed to RSG1-CAF and RSG3-CAF. Quantitation and analysis were similar to those performed for the triple co-culture experiments. Data represents the mean of three different experiments performed in triplicate.

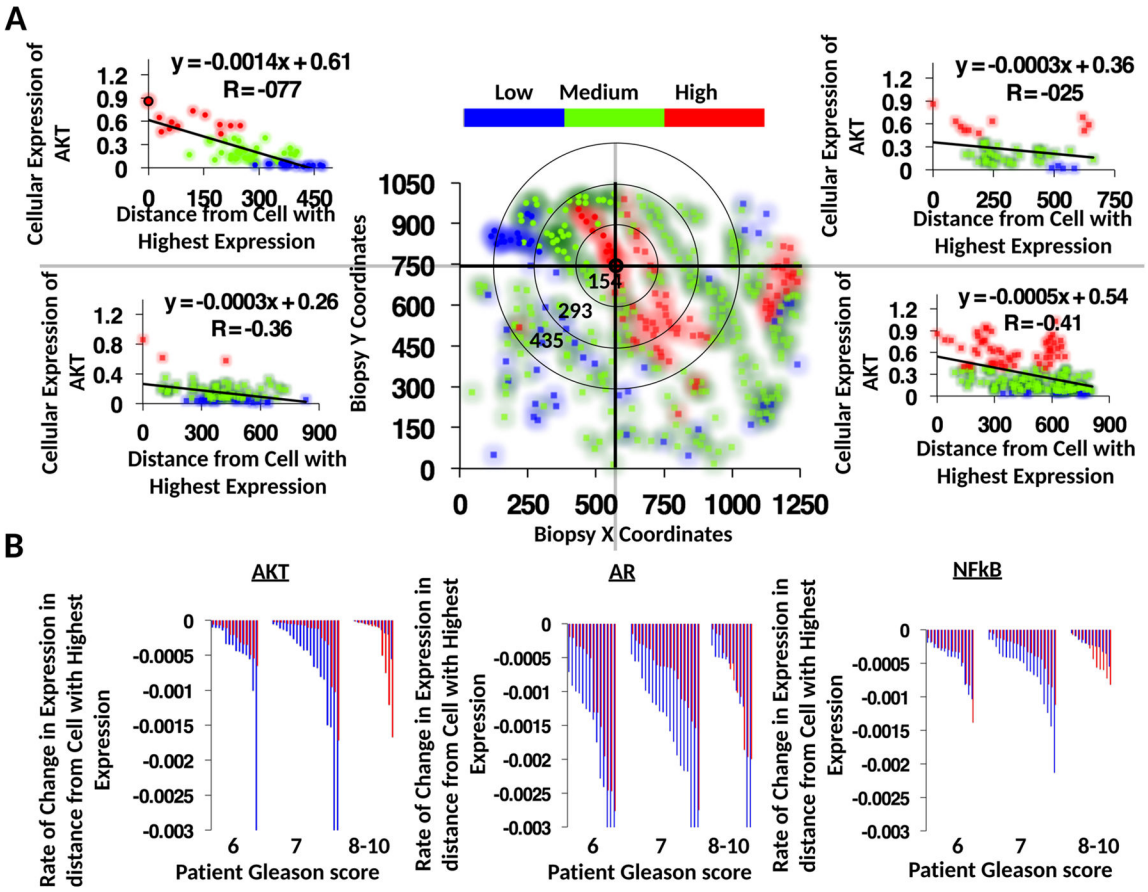

Extended Data Fig. 5 | Calculating evolutionary gradients from patient biopsies.

Analysis of triple stained tissue samples (Gleason 7 with RSG1) illustrating our approach to identify the most statistically significant evolutionary gradient in AKT expression. To identify the most significant gradient across a given biopsy, we analyzed the rate of change in expression through space starting from the cell with highest individual level of expression. Slope was calculated across radial distance from the cell with highest expression in the biopsy, in the example shown here, coordinates (575,746) (**a**). Analysis was performed on patients with RSG1 and compared to RSG3 in each Gleason category (**b**) showing the most significant slope per patient for the 3 molecular markers, AKT (left), AR (middle) and NF-B (phospho-p65, right). The larger the slope the more quickly expression changes with distance from the highest expressing cell. per patient for the 3 molecular markers, AKT (left), AR (middle) and NF-B (phospho-p65, right). The larger the slope the more quickly expression changes with distance from the highest expressing cell.

Supplementary Material

Refer to Web version on PubMed Central for supplementary material.

Acknowledgements

A.R.A.A., G.A. and S.W.H. gratefully acknowledge National Cancer Institute funding for this work through grant no. U01CA151924.

Data availability

All clinical data used was de-identified. All clinical data elements exist at Baylor College of Medicine, but the authors no longer have direct access to them. Contact G. Ayala to discuss clinical data access.

Code availability

The code used to produce all the simulations in the paper is available at the https://github.com/MathOnco/PCASim github repository.

References

1. Strand DW, Franco OE, Basanta D, Anderson ARA & Hayward SW Perspectives on tissue interactions in development and disease. Curr. Mol. Med 10, 95–112 (2010). [PubMed: 20205682]
2. Simon-Assmann P, Spenle C, Lefebvre O & Kedinger M The role of the basement membrane as a modulator of intestinal epithelial-mesenchymal interactions. Prog. Mol. Biol. Transl. Sci 96, 175–206 (2010). [PubMed: 21075345]
3. Parmar H & Cunha GR Epithelial-stromal interactions in the mouse and human mammary gland in vivo. Endocr. Relat. Cancer 11, 437–458 (2004). [PubMed: 15369447]
4. Sugimoto H, Mundel TM, Kieran MW & Kalluri R Identification of fibroblast heterogeneity in the tumor microenvironment. Cancer Biol. Ther 5, 1640–1646 (2006). [PubMed: 17106243]
5. Orimo A. et al. Stromal fibroblasts present in invasive human breast carcinomas promote tumor growth and angiogenesis through elevated SDF-1/CXCL12 secretion. Cell 121, 335–348 (2005). [PubMed: 15882617]
6. Tuxhorn JA, Ayala GE & Rowley DR Reactive stroma in prostate cancer progression. J. Urol 166, 2472–2483 (2001). [PubMed: 11696814]
7. Tuxhorn JA, McAlhany SJ, Dang TD, Ayala GE & Rowley DR Stromal cells promote angiogenesis and growth of human prostate tumors in a differential reactive stroma (DRS) xenograft model. Cancer Res. 62, 3298–3307 (2002). [PubMed: 12036948]
8. Ayala G. et al. Reactive stroma as a predictor of biochemical-free recurrence in prostate cancer. Clin. Cancer Res 9, 4792–4801 (2003). [PubMed: 14581350]
9. Olumi AF et al. Carcinoma-associated fibroblasts direct tumor progression of initiated human prostatic epithelium. Cancer Res. 59, 5002–5011 (1999). [PubMed: 10519415]
10. Franco OE et al. Altered TGF-β signaling in a subpopulation of human stromal cells promotes prostatic carcinogenesis. Cancer Res. 71, 1272–1281 (2011). [PubMed: 21303979]
11. Kiskowski MA et al. Role for stromal heterogeneity in prostate tumorigenesis. Cancer Res. 71, 3459–3470 (2011). [PubMed: 21444670]
12. Bremnes RM et al. The role of tumor stroma in cancer progression and prognosis: emphasis on carcinoma-associated fibroblasts and non-small cell lung cancer. J. Thorac. Oncol 6, 209–217 (2011). [PubMed: 21107292]
13. Tuxhorn JA et al. Reactive stroma in human prostate cancer: induction of myofibroblast phenotype and extracellular matrix remodeling. Clin. Cancer Res 8, 2912–2923 (2002). [PubMed: 12231536]
14. Levesque C & Nelson PS Cellular constituents of the prostate stroma: key contributors to prostate cancer progression and therapy resistance. Cold Spring Harb. Perspect. Med 8, a030510 (2018). [PubMed: 28490538]
15. Yanagisawa N. et al. Reprint of: Stromogenic prostatic carcinoma pattern (carcinomas with reactive stromal grade 3) in needle biopsies predicts biochemical recurrence-free survival in patients after radical prostatectomy. Hum. Pathol 39, 282–291 (2008). [PubMed: 18206496]
16. Diaz De Vivar A. et al. Histologic features of stromogenic carcinoma of the prostate (carcinomas with reactive stroma grade 3). Hum. Pathol 63, 202–211 (2017). [PubMed: 28315427]

17. Ayala GE et al. Determining prostate cancer-specific death through quantification of stromogenic carcinoma area in prostatectomy specimens. Am. J. Pathol 178, 79–87 (2011). [PubMed: 21224046]
18. San Martin R. et al. Recruitment of CD34^{+} fibroblasts in tumor-associated reactive stroma: the reactive microvasculature hypothesis. Am. J. Pathol 184, 1860–1870 (2014). [PubMed: 24713391]
19. Potosky AL et al. Five-year outcomes after prostatectomy or radiotherapy for prostate cancer: the prostate cancer outcomes study. J. Natl Cancer Inst 96, 1358–1367 (2004). [PubMed: 15367568]
20. Penson DF et al. General quality of life 2 years following treatment for prostate cancer: what influences outcomes? Results from the Prostate Cancer Outcomes Study. J. Clin. Oncol 21, 1147–1154 (2003). [PubMed: 12637483]
21. Pound CR et al. Natural history of progression after PSA elevation following radical prostatectomy. JAMA 281, 1591–1597 (1999). [PubMed: 10235151]
22. Han M, Partin AW, Pound CR, Epstein JI & Walsh PC Long-term biochemical disease-free and cancer-specific survival following anatomic radical retropubic prostatectomy. The 15-year Johns Hopkins experience. Urol. Clin. North Am 28, 555–565 (2001). [PubMed: 11590814]
23. Roehl KA, Han M, Ramos CG, Antenor JA & Catalona WJ Cancer progression and survival rates following anatomical radical retropubic prostatectomy in 3,478 consecutive patients: long-term results. J. Urol 172, 910–914 (2004). [PubMed: 15310996]
24. Hull GW et al. Cancer control with radical prostatectomy alone in 1,000 consecutive patients. J. Urol 167, 528–534 (2002). [PubMed: 11792912]
25. Amling CL et al. Long-term hazard of progression after radical prostatectomy for clinically localized prostate cancer: continued risk of biochemical failure after 5 years. J. Urol 164, 101–105 (2000). [PubMed: 10840432]
26. Moul JW Treatment of PSA only recurrence of prostate cancer after prior local therapy. Curr. Pharm. Des 12, 785–798 (2006). [PubMed: 16515495]
27. Harrington S, Lee J, Colon G & Alappattu M Oncology section EDGE task force on prostate cancer: a systematic review of outcome measures for health-related quality of life. Rehabil. Oncol 34, 27–35 (2016). [PubMed: 27134804]
28. Basanta D. et al. The role of transforming growth factory-β-mediated tumor-stroma interactions in prostate cancer progression: an integrative approach. Cancer Res. 69, 7111–7120 (2009). [PubMed: 19706777]
29. Basanta D. et al. Investigating prostate cancer tumour-stroma interactions: clinical and biological insights from an evolutionary game. Br. J. Cancer 106, 174–181 (2012). [PubMed: 22134510]
30. Flach EH, Rebecca VW, Herlyn M, Smalley KSM & Anderson ARA Fibroblasts contribute to melanoma tumor growth and drug resistance. Mol. Pharm 8, 2039–2049 (2011). [PubMed: 22067046]
31. Kim E. et al. Senescent fibroblasts in melanoma initiation and progression: an integrated theoretical, experimental, and clinical approach. Cancer Res. 73, 6874–6885 (2013). [PubMed: 24080279]
32. Araujo A, Cook LM, Lynch CC & Basanta D An integrated computational model of the bone microenvironment in bone-metastatic prostate cancer. Cancer Res. 74, 2391–2401 (2014). [PubMed: 24788098]
33. Picco N, Sahai E, Maini PK & Anderson AR Integrating models to quantify environment-mediated drug resistance. Cancer Res. 77, 5409–5418 (2017). [PubMed: 28754669]
34. Kaznatcheev A, Peacock J, Basanta D, Marusyk A & Scott JG Fibroblasts and alectinib switch the evolutionary games played by non-small cell lung cancer. Nat. Ecol. Evol 3, 450–456 (2019). [PubMed: 30778184]
35. Kim Y & Othmer HG A hybrid model of tumor-stromal interactions in breast cancer. Bull. Math. Biol 75, 1304–1350 (2013). [PubMed: 23292359]
36. Martin NK, Gaffney EA, Gatenby RA & Maini PK Tumour-stromal interactions in acid-mediated invasion: a mathematical model. J. Theor. Biol 267, 461–470 (2010). [PubMed: 20816684]
37. McKenney JK et al. Histologic grading of prostatic adenocarcinoma can be further optimized: analysis of the relative prognostic strength of individual architectural patterns in 1275 patients

from the canary retrospective cohort. Am. J. Surg. Pathol 40, 1439–1456 (2016). [PubMed: 27635949]

38. Quaranta V, Weaver AM, Cummings PT & Anderson ARA Mathematical modeling of cancer: the future of prognosis and treatment. Clin. Chim. Acta 357, 173–179 (2005). [PubMed: 15907826]
39. Anderson ARA A hybrid mathematical model of solid tumour invasion: the importance of cell adhesion. Math. Med. Biol 22, 163–186 (2005). [PubMed: 15781426]
40. Rejniak KA & Anderson ARA Hybrid models of tumor growth. Wiley Interdiscip. Rev. Syst. Biol. Med 3, 115–125 (2011). [PubMed: 21064037]
41. Raman D, Baugher PJ, Thu YM & Richmond A Role of chemokines in tumor growth. Cancer Lett. 256, 137–165 (2007). [PubMed: 17629396]
42. Grivennikov SI, Greten FR & Karin M Immunity, inflammation, and cancer. Cell 140, 883–899 (2010). [PubMed: 20303878]
43. Fluge O. et al. Expression of EZH2 and Ki-67 in colorectal cancer and associations with treatment response and prognosis. Br. J. Cancer 101, 1282–1289 (2009). [PubMed: 19773751]
44. Ao M. et al. Cross-talk between paracrine-acting cytokine and chemokine pathways promotes malignancy in benign human prostatic epithelium. Cancer Res. 67, 4244–4253 (2007). [PubMed: 17483336]
45. Maru N, Ohori M, Kattan MW, Scardino PT & Wheeler TM Prognostic significance of the diameter of perineural invasion in radical prostatectomy specimens. Hum. Pathol 32, 828–833 (2001). [PubMed: 11521227]
46. Li R. et al. Prognostic value of Akt-1 in human prostate cancer: a computerized quantitative assessment with quantum dot technology. Clin. Cancer Res 15, 3568–3573 (2009). [PubMed: 19417030]
47. Li R. et al. High level of androgen receptor is associated with aggressive clinicopathologic features and decreased biochemical recurrence-free survival in prostate: cancer patients treated with radical prostatectomy. Am. J. Surg. Pathol 28, 928–934 (2004). [PubMed: 15223964]
48. Altman DG, Lausen B, Sauerbrei W & Schumacher M Dangers of using “optimal” cutpoints in the evaluation of prognostic factors. J. Natl Cancer Inst 86, 829–835 (1994). [PubMed: 8182763]
49. Dakhova O. et al. Global gene expression analysis of reactive stroma in prostate cancer. Clin. Cancer Res 15, 3979–3989 (2009). [PubMed: 19509179]
50. Hayashi N & Cunha GR Mesenchyme-induced changes in the neoplastic characteristics of the Dunning prostatic adenocarcinoma. Cancer Res. 51, 4924–4930 (1991). [PubMed: 1893381]
51. Wheeler TM & Lebovitz RM Fresh tissue harvest for research from prostatectomy specimens. Prostate 25, 274–279 (1994). [PubMed: 7526353]
52. Therneau TM & Grambsch PM Modeling Survival Data: Extending the Cox Model (Springer, 2000).
53. Gronnesby JK & Borgan Ø. A method for checking regression models in survival analysis based on the risk score. Lifetime Data Anal. 2, 315–328 (1996). [PubMed: 9384628]
54. Grambsch PM, Therneau TM & Fleming TR Diagnostic plots to reveal functional form for covariates in multiplicative intensity models. Biometrics 51, 1469–1482 (1995). [PubMed: 8589234]
55. Pepe MS, Janes H, Longton G, Leisenring W & Newcomb P Limitations of the odds ratio in gauging the performance of a diagnostic, prognostic, or screening marker. Am. J. Epidemiol 159, 882–890 (2004). [PubMed: 15105181]
56. Wu HC et al. Derivation of androgen-independent human LNCaP prostatic cancer cell sublines: role of bone stromal cells. Int. J. Cancer 57, 406–412 (1994). [PubMed: 8169003]

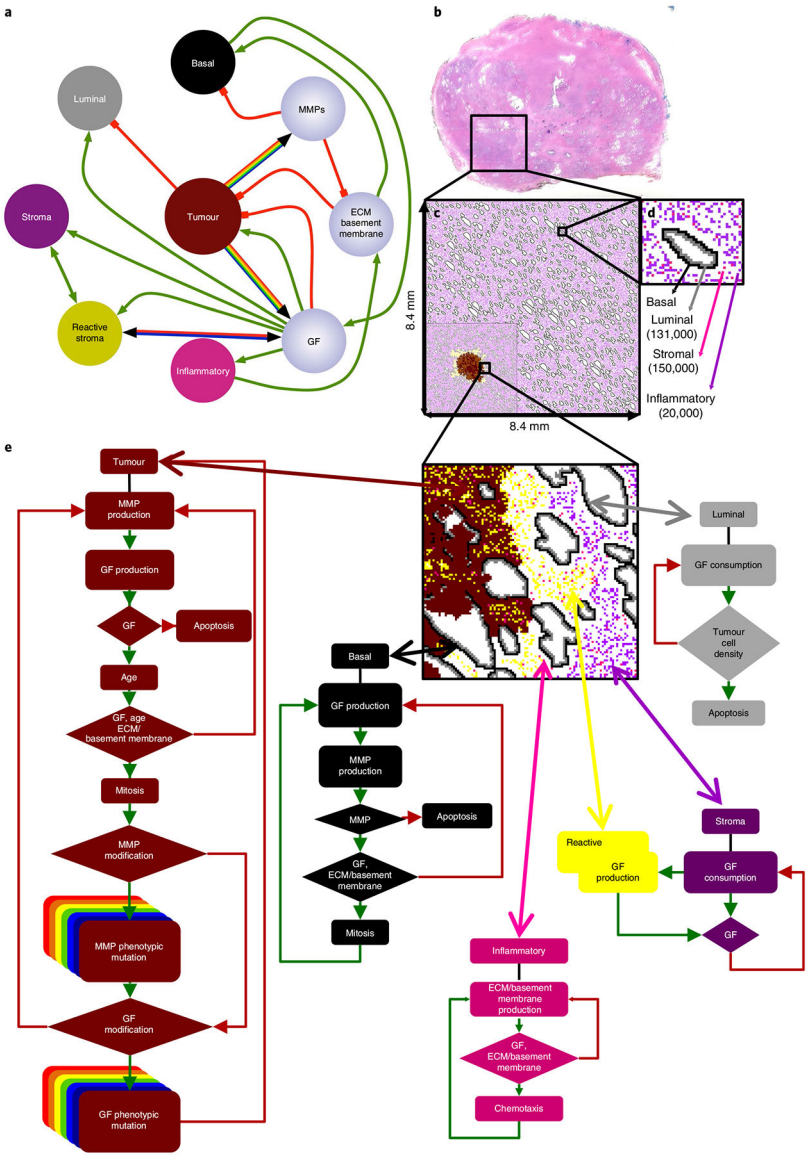

Fig. 1 |. In silico multiscale model of the prostate peripheral zone.

a, Interaction network of key model variables. Interactions between cells (coloured nodes) and microenvironmental variables (lilac nodes) are represented as either green (positive) or red (negative) connections. Multicoloured connectivity represents the spectrum of possible tumour phenotypes with different levels of growth factor and MMP production. Bicoloured connectivity represents two different degrees of stromal reactivity. **b**-**d**, In silico reconstruction of the normal prostate peripheral zone tissue. **b**, Histopathological slide of the whole normal prostate, highlighting the peripheral zone, filled with epithelial acini surrounded by stroma (magenta). **c**, In silico representation of the complete peripheral zone, including ductal structures and cellular densities that mimic normal anatomy. This constitutes the domain where all simulations were performed. The inset on the bottom left is an example of a sample simulation **d**, Representation of a single reconstructed duct and the surrounding stroma, as well as the total number of cell types. **e**, Cell decision flow charts for

each cell type in the model. The phenotypic behaviour of an individual cell is based on the interaction between the cell and the local microenvironment. GF, growth factor.

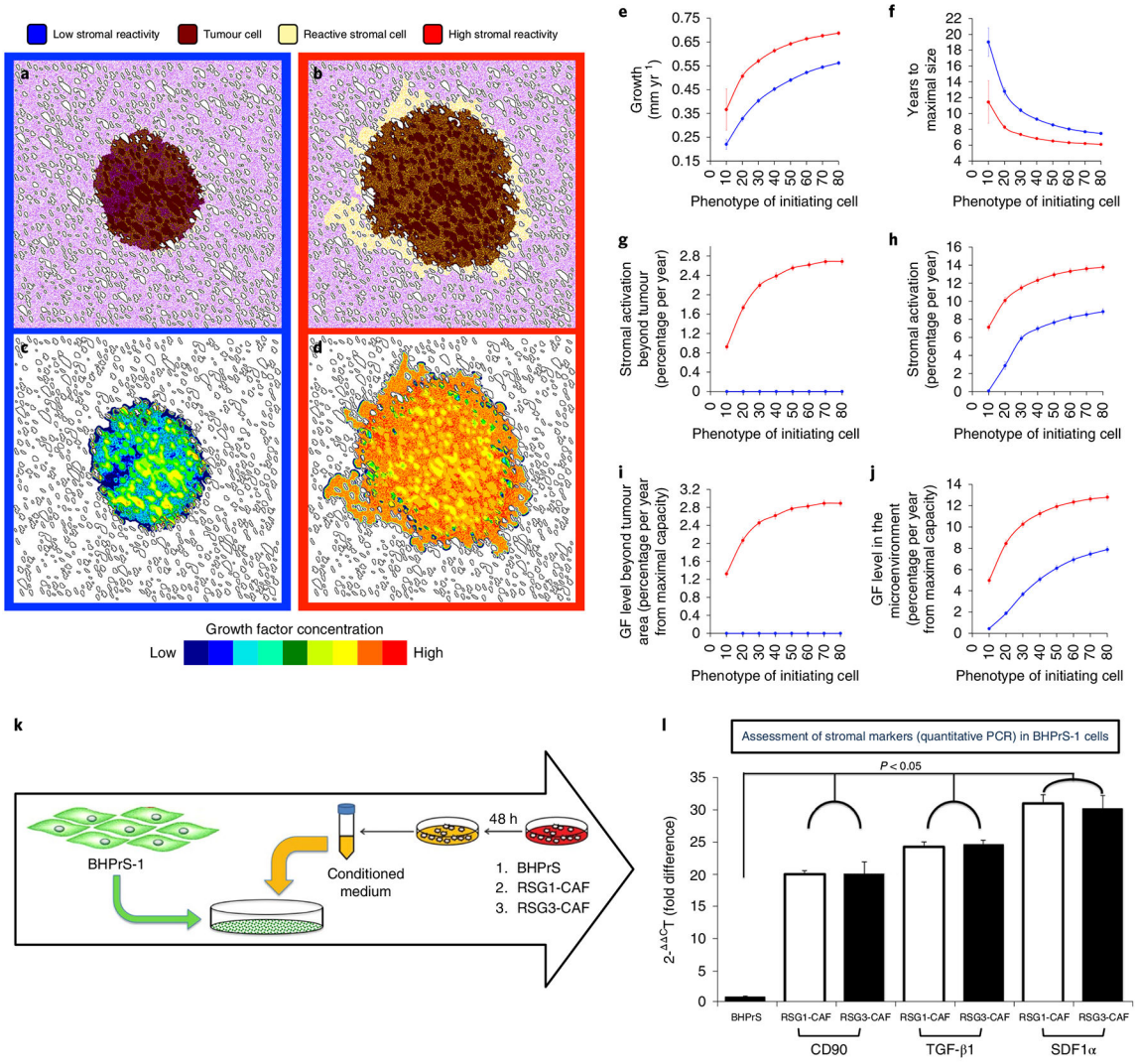

Fig. 2 | Change in stromal reactivity phenotypes, tumour growth and invasiveness.

a-d, Six years of simulated tumour growth, initialized with a tumour cell producing low levels of growth factors (20% of the maximal simulated cell production capacity) under two different microenvironmental conditions: low stromal reactivity (**a,c**, blue frames and lines) or high stromal reactivity (**b,d**, red frames and lines). **a** and **b** show tumour cell spatial distribution (brown) with normal stroma (purple) and reactive stroma (yellow); **c** and **d** show the resulting spatial distributions of growth factor concentration for tumours **a** and **b**, respectively. **e-j**, Different tumour metric distributions over eight initiating phenotypes (ranging from 10% to 80% of the maximal simulated cell growth factor production capacity) in high (red) and low (blue) stromal reactivity environments averaged over 100 simulations per phenotype (error bars represent mean ± s.d.). **e**, Average growth of the tumour. **f**, Time to achieve maximal size (reach the edge of the tissue domain). **g,h**, Percentage of stromal activation within (**g**) and beyond (**h**) the tumour varied with the phenotype of the tumour-initiating cells and with the stromal reactivity. **i,j**, The concentration of growth factor found in the microenvironment beyond (**i**) and within (**j**) the tumour parallels stromal activation. **k**,

To assess the ability of reactive stroma to activate benign stroma cells, the human prostate stromal cell line BHPrS1 was cultured in the presence of conditioned medium from either BHPrS1, RSG1-CAF or RSG3-CAF for 4 weeks. **l**, At the end of the experiment, expression of CD90, TGF-β1 and SDF1α (all putative activated stromal markers) was determined by quantitative PCR. Conditioned media from RSG1-CAF and RSG3-CAF elicited a similar and significant increase in the levels of these mRNAs compared to medium conditioned by the functionally normal BHPrS1 cell line. Relative levels of mRNA are shown compared to a control standardized to a mean value of one. Error bars represent s.d. In all three cases, the marker mRNAs are increased markedly by conditioned medium ($P < 0.05$; ANOVA) but there was no difference in effect between conditioned medium from RSG1- or RSG3-derived fibroblasts.

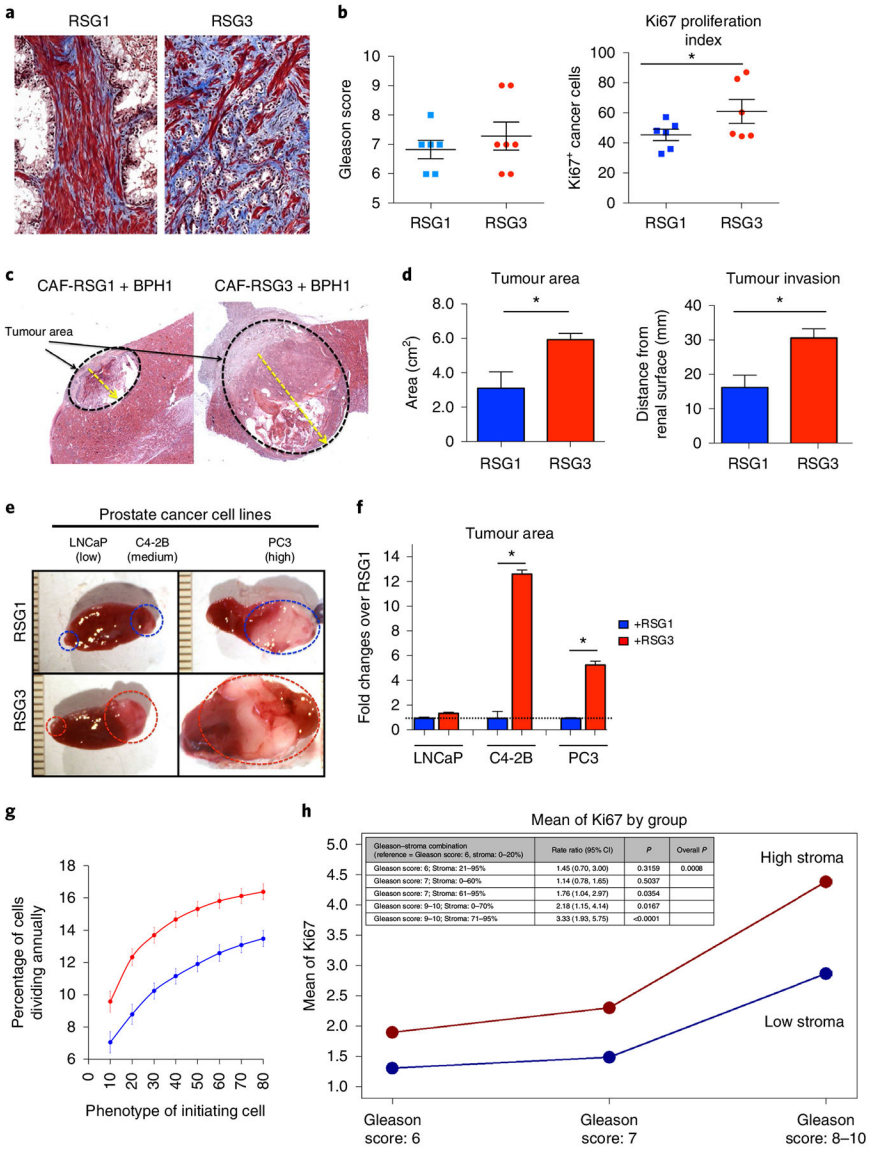

Fig. 3 | In vivo stromogenic grade is linked to tumour growth and invasion but not to Gleason grade.

a, Representative images of stromogenic response in PCa from two different patients showing RSG1 (left) and RSG3 (right). Note the intense and high percentage of reactive stroma (blue) depicting increased collagen deposition in the RSG3 sample. **b**, A total of 23 patients were categorized according to their Gleason score (left). No correlation was found between Gleason score and RSG. However, cancer cells surrounded by RSG3 stroma had increased proliferation (number of Ki67+ stained cells) compared to RSG1 as determined by *t*-test comparison (*$P < 0.05$). **c**, Response of an initiated reporter epithelial cell line (BPH1) to CAFs is a function of the RSG status of the tumour source of the CAFs. Low magnification of CAF combined with BPH1 cells in vivo. Both RSG1-CAF and RSG3-CAF promoted malignant transformation. **d**, Quantitation of tumour area and invasion revealed increased growth and aggressiveness in RSG3-CAF compared to RSG1-CAF (*t*-test analysis performed to compare differences between groups, three different

experiments each performed in triplicate; $P < 0.01$ in both cases). Response of epithelial cells to CAFs is a product of both the epithelial and stromal components of the tumour. **e**, Gross picture of the PCa cell lines LNCaP, C4-2B and PC-3 cells tissue recombinants with RSG1- and RSG3-CAFs. Six recombinants per group were grafted using 12 animals. **f**, Fold change analysis of PCa cell lines combined with RSG-CAFs in a tissue recombinant show significant increased growth in the presence of RSG3 compared to RSG1 in C4-2B and PC-3 but not LnCaP cells (*t*-test analysis performed to compare differences between groups, three different experiments each performed in triplicate; $P < 0.01$ for C4-2B and PC3). **g**, Tumour cell division rate calculated from our in silico model simulations over 8 different initiating phenotypes in high (red) and low (blue) stromal reactivity environments (averaged over 100 simulations; error bars represent mean ± s.d.). **h**, The proliferation rate of cancer cells, as measured by Ki67, was significantly higher in stromogenic than non-stromogenic cancers, in all Gleason categories based on the Poisson regression model.

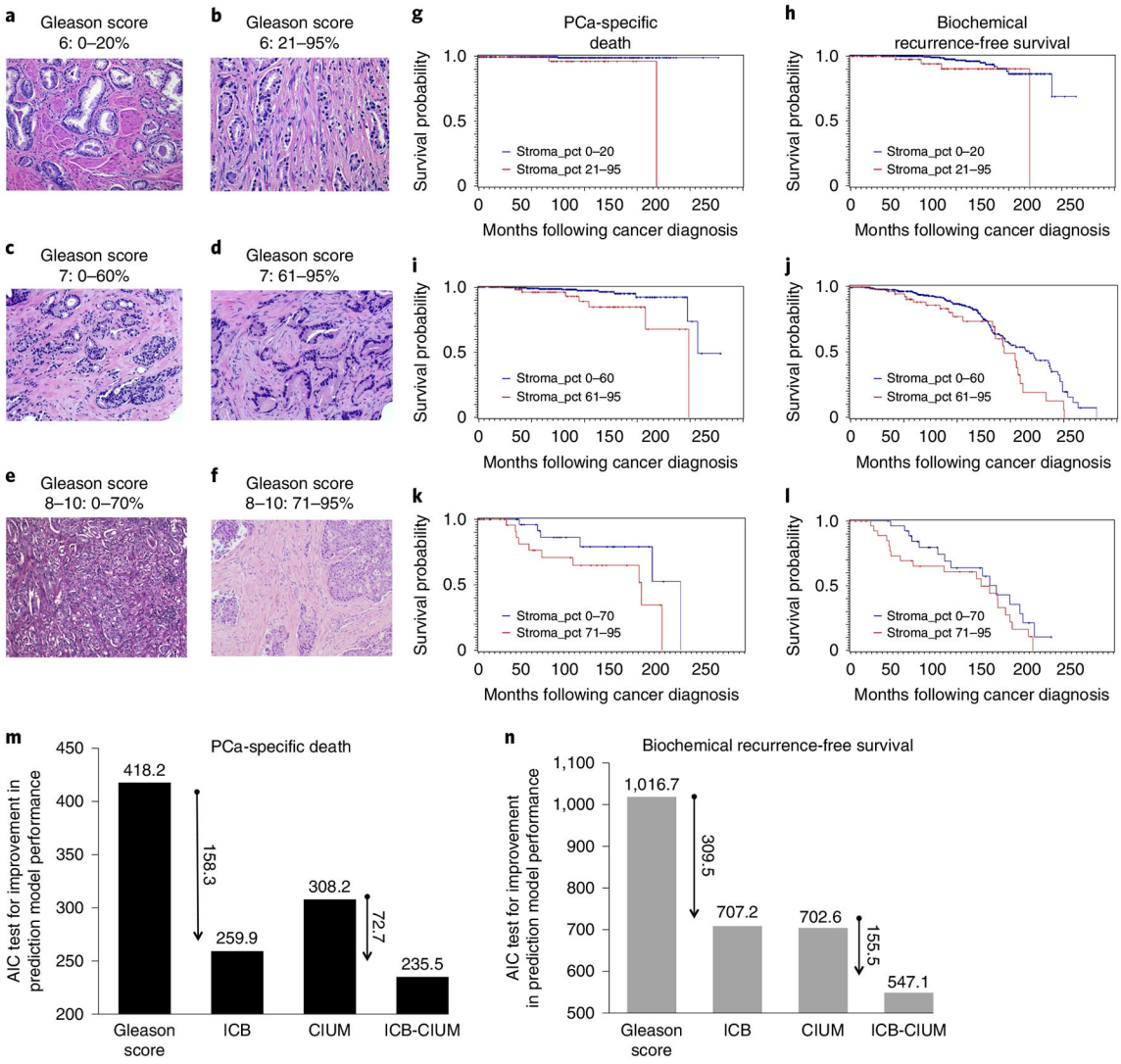

Fig. 4 |. The ICB stratifies all Gleason grades in a cohort of 1,291 PCa patients with over 20 years of follow-up.

a,b, Histology of a Gleason-score-6 cancer without stromal response (**a**) compared to a Gleason-score-6 cancer with exuberant stromogenic response (RSG3) (**b**). **g,h**, Patients with more than 20% of the tumour having an RSG3 pattern were associated with increased PCa-specific death (**g**, $P = 0.0008$) and biochemical recurrence (**h**, $P = 0.0597$). **c,d**, Histological representations for Gleason-score-7 cancers without reactive stroma (**c**) and with RSG3 (**d**). **i,j**, In Gleason-score-7 patients, the cut-off for statistical significance is 60% of the tumour having an RSG3 pattern (**i**, PCa-specific death, $P = 0.004$; **j**, biochemical recurrence, $P = 0.0341$). **e,f**, High-Gleason-score cancers (Gleason score, 8-10) can grow in solid masses (**e**) or embedded in RSG3 (**f**). **k,l**, The cut-off in this category is higher at 70% (**k**, PCa-specific death, $P = 0.0716$; **l**, biochemical recurrence, $P = 0.1738$). An AIC test was used to compare different predictive models of PCa-specific death and recurrence-free survival. CIUM, clinical in use methodology: Gleason score, seminal vesicle invasion, extra-capsular extension and PSA. **m,n**, The AIC model for PCa-specific death-free survival (**m**) and

biochemical recurrence-free survival (**n**) show the much-improved performance of the ICB compared to standard of care. The preferred model is the one with the lowest AIC value. **g-l**, A log-rank test was used.

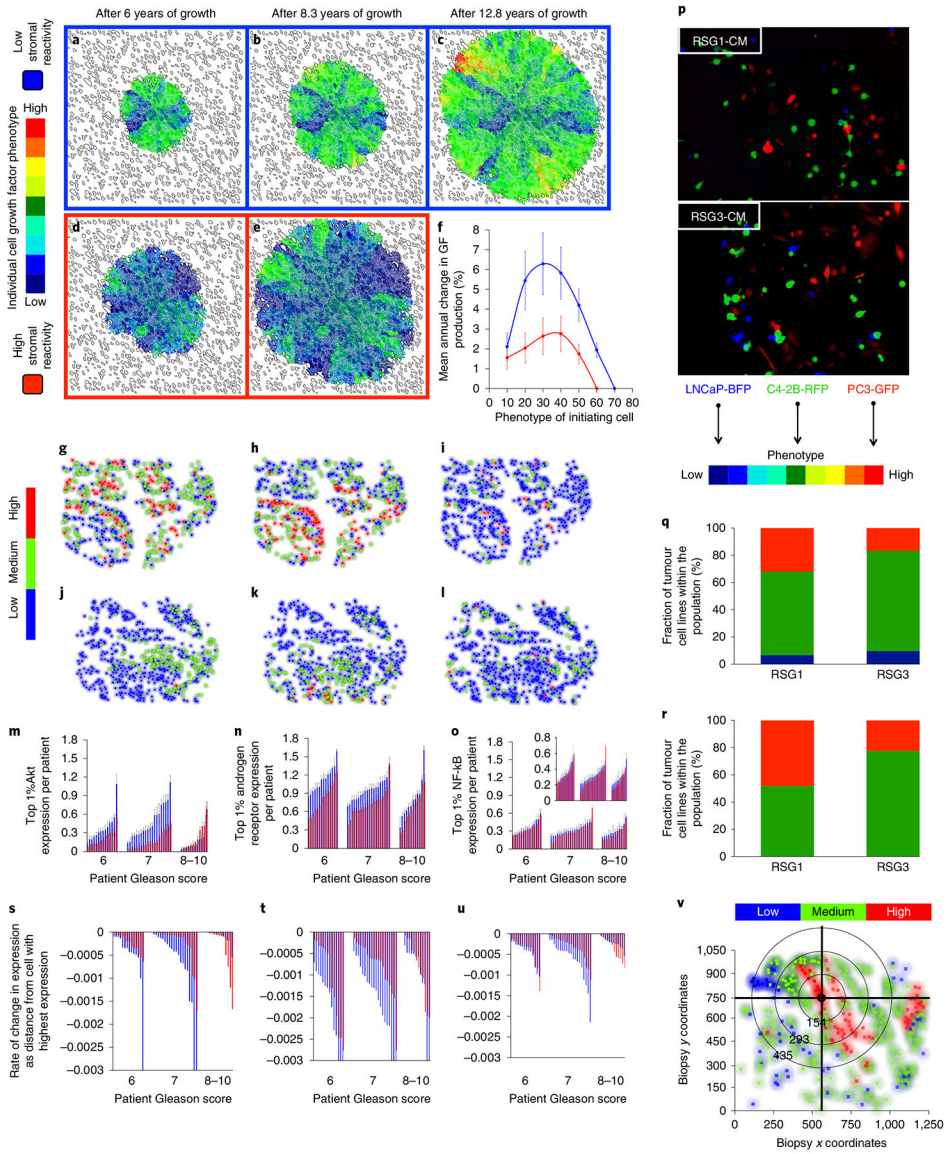

Fig. 5 | Stromal reactivity drives tumour cell evolution and progression: in silico and clinical analysis.

a-e, Evolution of tumour cell phenotypes through space and time (6-12.8 years) under low (blue) and high (red) stromal reactivity conditions (this figure extends the timescale of Fig. 2a-d). The heatmap shows tumour cell phenotype (growth factor production) distribution in low (**a-c**) and high stromal reactivity (**d,e**) after 6 (**a,d**), 8.3 (**b,e**) and 12.8 (**c**) years of growth. **f**, Tumour cell phenotypic change in growth factor production from 8 different initiating phenotypes in high (red) and low (blue) stromal reactivity environments (the average change and s.d. across 300 simulations per initiating phenotype) is shown. **g-l**, Representative samples of triple-immunostained biopsies for three well-established PCa molecular regulators—phosphorylated Akt (**g,j**); androgen receptor (**h,k**); and the central inflammatory regulator NF-κB (**i,l**)—from two patients, one with RSG1 (**g-i**) and the other with RSG3 (**j-l**); levels of expression were classified as low (blue), medium (green) or high (red). **m-o**, Single-cell quantitative analysis of triple-immunostained tissue sections

for patients with RSG1 (blue) versus RSG3 (red) in each Gleason category for the three molecular markers, Akt (**m**), androgen receptor (**n**) and NF-κB (phospho-p65, **o**). The top 1% of gene expression in cells from each of the patient's biopsies are shown (subset of the tumour cell population that would be under the greater selection pressure); each individual bar represents the average (and s.d.) for a single patient over many cells. The PCa cell lines LNCaP-BFP (blue), C4-2B-RFP (green) and PC-3-GFP (red) were cultured in the presence of conditioned medium from either NPF, RSG1-CAF or RSG3-CAF for 4 weeks. **p**, Representative images for each group are shown (cells are false coloured for internal consistency of illustrations). **q,r**, Quantitation of individual cell populations was determined by fluorescence-activated cell sorting analysis and shows the fraction of each tumour cell line, LNCaP-BFP (blue), C4-2B-RFP (green) and PC-3-GFP (red), in RSG1-CAF or RSG3-CAF conditioned medium. To identify the most significant evolutionary gradient in expression across a given biopsy, we analysed the rate of change in expression through space starting from the cell with the highest individual level of expression. Each sample was split into four different sections, with the origin of this split being the highest expressing cell in the example shown (coordinates, 575,746) (**v**) (see Extended Data Fig. 5 for more detail). The slope from that cell to the edge of the biopsy in terms of radial distance was then calculated. The most statistically significant slope was the one assigned to that specific patient. **s-u**, This analysis was performed on patients with RSG1 and compared to RSG3 in each Gleason category showing the most significant slope per patient for the three molecular markers, Akt (**s**), androgen receptor (**t**) and NF-κB (phospho-p65) (**u**). The larger the slope the more quickly expression changes with distance from the highest expressing cell. In **m-o** and **s-u**, 14 RSG1 and 14 RSG3 Gleason-score-6 patients; 20 RSG1 and 20 RSG3 Gleason-score-7 patients; and 12 RSG1 and 12 RSG3 Gleason-score-8-10 patients were analysed.

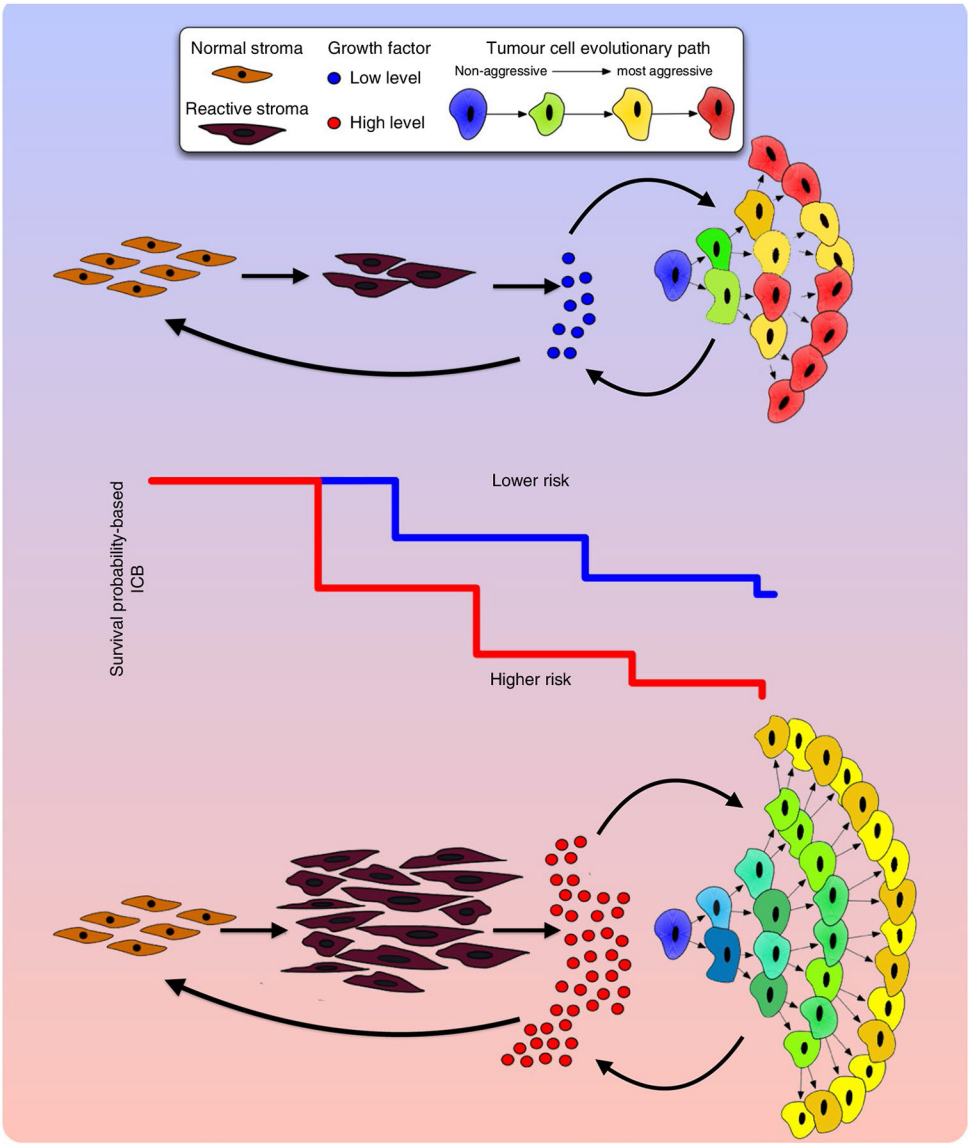

Fig. 6 |. Interactions between tumour cells and stroma shape the evolutionary dynamics of PCa and drive overall tumour aggressiveness.

Growth factor signalling is essential to both tumour and reactive stroma. Limited availability of growth factors leads to an increased competition between tumour and stromal cells. This competition results in slower tumour growth (lower risk estimation) but also increased selection and more rapid evolution (leading to a more heterogeneous population). In contrast, where growth factor availability is not limiting, there are more mutualistic interactions between tumour and stroma. This situation results in faster growing tumours (higher risk estimation) but, paradoxically, weaker selection pressure leading to less aggressive tumour cells (and a less heterogeneous population). Therefore, evolution of the most malignant phenotypes in a tumour cell population is not necessarily consistent tumour growth and invasion since it is modulated by the stromal response. In addition, tumour aggressiveness, as defined by the Gleason score, is differentially modulated by stromal response. These different risk estimations and evolutionary dynamics (and tumour

heterogeneity) mean that the overall behaviour of patient tumours is driven by both tumour cells (Gleason score) and the stromal response of the host (ICB).

Table 1 |

Multivariable association between iCB and risk of biochemical recurrence and PCa-specific death based on the Cox proportional hazards model

Variable	Adjusted hazard ratio (95% confidence interval)	*P*
Biochemical recurrence		
ICB (reference: Gleason score 6/RSG3 0-20)		<0.0001
Gleason score 6/RSG3 21-95	2.41 (0.67, 8.62)	0.1763
Gleason score 7/RSG3 0-60	3.2 (1.70, 6.04)	0.0003
Gleason score 7/RSG3 61-95	4.32 (2.05, 9.10)	0.0001
Gleason score 8-10/RSG3 0-70	3.25 (1.42, 7.44)	0.0054
Gleason score 8-10/RSG3 71-95	7.29 (3.37, 15.77)	<0.0001
Extra-capsular extension versus none	1.50 (0.95, 2.38)	0.0834
Seminal vesicle invasion versus none	1.35 (0.93, 1.96)	0.1165
Margins versus none	2.24 (1.55, 3.24)	<0.0001
Lymph node status versus none	2.82 (1.91, 4.16)	<0.0001
log(preoperative PSA) >1.9 versus ≤1.9	1.80 (1.19, 2.72)	0.0056
PCa-specific death		
ICB (reference: Gleason score 6/RSG3 0-20)		<0.0001
Gleason score 6/RSG3 21-95	7.89 (0.47, 131.5)	0.1499
Gleason score 7/RSG3 0-60	5.64 (0.68, 46.58)	0.1083
Gleason score 7/RSG3 61-95	12.69 (1.38, 117.0)	0.025
Gleason score 8-10/RSG3 0-70	18.6 (1.85, 186.8)	0.013
Gleason score 8-10/RSG3 71-95	55.82 (6.22, 501.0)	0.0003
Extra-capsular extension versus none	1.94 (0.52, 7.33)	0.3265
Seminal vesicle invasion versus none	2.81 (1.26, 6.26)	0.0118
Margins versus none	1.26 (0.50, 3.14)	0.6242
Lymph node status versus none	1.84 (0.83, 4.05)	0.1321
log(preoperative PSA) >1.9 versus ≤1.9	0.89 (0.40, 1.96)	0.7698